

Is there Evidence for Flat Cores in the Halos of Dwarf Galaxies?: The Case of NGC 3109 and NGC 6822

Octavio Valenzuela¹, George Rhee², Anatoly Klypin³, Fabio Governato¹,
Gregory Stinson¹, Thomas Quinn¹, James Wadsley⁴

¹ *Department of Astronomy, University of Washington Seattle, USA, WA 9819*

² *University of Nevada, Department of Physics Box 454002, Las Vegas, NV 89154-4002*

³ *Astronomy Department, New Mexico State University, Box 30001, Department 4500, Las Cruces, NM 88003-0001*

⁴ *Department of Physics and Astronomy, McMaster University, Hamilton, Ontario L8S 2M1, Canada*

ABSTRACT

Two well studied dwarf galaxies – NGC 3109 and NGC 6822 – present some of the strongest observational support for a flat core at the center of galactic dark matter (DM) halos. We use detailed cosmologically motivated numerical models to investigate the systematics and the accuracy of recovering parameters of the galaxies. Some of our models match the observed structure of the two galaxies remarkably well. Our analysis shows that the rotation curves of these two galaxies are instead quite compatible with their DM halos having steep cuspy density profiles. The rotation curves in our models are measured using standard observational techniques, projecting velocities along the line of sight of an artificial observer and performing a tilted ring analysis. The models reproduce the rotation curves of both galaxies, the disk surface brightness profiles as well as the profile of isophotal ellipticity and position angle. The models are centrally dominated by baryons; however, the dark matter component is globally dominant. The simulated disk mass is marginally consistent with a stellar mass-to-light ratio in agreement with the observed colors and the detected gaseous mass. We show that non-circular motions combined with gas pressure support and projection effects results in a large underestimation of the circular velocity in the central ~ 1 kpc region, creating the illusion of a constant density core. Although the systematic effects mentioned above are stronger in barred systems, they are also present in axisymmetric disks. Our results strongly suggest that there is no contradiction between the observed rotation curves in dwarf galaxies and the cuspy central dark matter density profiles predicted by Cold Dark Matter models.

Subject headings: Cosmology:Dark Matter¹, Galaxies:Dwarf, Galaxies:Individual NGC 6822, NGC 3109, Local Group, Galaxies:Halos, Galaxies:Kinematics and Dynamics

1. Introduction

Cosmological models based on the inflationary paradigm, Cold Dark Matter (CDM), and dark energy (Λ CDM) are very successful in explaining the large scale structure of the Universe (Spergel et al. 2003). However, it has been widely argued that Λ CDM models face a number of challenges at galactic scales (Moore 1994; Flores & Primack 1994; de Blok & McGaugh 1997; McGaugh & de Blok 1998; Moore 2001; Ostriker & Steinhardt 2003). One of the most persistent problems is the apparent incompatibility of galaxy kinematics with the structure of dark matter halos predicted by cosmology. Cosmological N-body simulations predict halos with a central cusp (Navarro, Frenk, & White 1997, NFW). Because low surface brightness (LSB) and dwarf galaxies are considered dark matter dominated at all radii, it is expected that their dynamics provide an excellent benchmark for testing the structure of CDM halos. It has been claimed that cosmological halos disagree with the shallow dark matter density profiles inferred from the rotation curves of dwarf and LSB galaxies (Moore 1994; Flores & Primack 1994; Burkert 1995; de Blok & McGaugh 1997). The galaxies seem to favor dark matter halos that have a soft core while cosmological halos are cuspy. The analysis of the cusp-core controversy has motivated a large amount of discussion and work (e.g., Firmani et al. 2000; Avila-Reese et al. 2001; Swaters et al. 2003a,b; Salucci et al. 2003; Simon et al. 2005; Rhee et al. 2004).

Earlier, the beam smearing in radio observations was believed to be responsible for some discrepancy between the obser-

vations and the theory (van den Bosch, Robertson, Dalcanton, & de Blok 2000; van den Bosch & Swaters 2001). Later, high angular resolution observations (e.g., de Blok, Bosma & McGaugh 2003; Swaters et al. 2003b; Weldrake et al. 2003; Simon et al. 2005), produced mixed results. In some cases rotation curves could be fitted with cuspy CDM halos, in others they could not. Swaters et al. (2003b) concluded that in a statistical sense the observed population of LSB galaxies is consistent with cosmological predictions. Only some dwarf galaxies in their sample are clearly inconsistent with cuspy cosmological halos. Hayashi et al. (2004) arrived at similar conclusions. Blais-Ouellette, Amram, & Carignan (2001) presented mass models for a sample of dwarf galaxies. For example, the data for NGC 5585 are compatible with a cuspy dark matter halo. However, the halo concentration is small and the stellar mass-to-light ratio (M/L) is null. Swaters et al. (2003a) presented evidence for non-circular motions in the galaxy DDO 39. After applying simple corrections to the rotation curve, the galaxy appears compatible with a cuspy dark matter halo assuming a (M/L) equal to one, but still favoring a relatively low concentration.¹

Rhee et al. (2004) showed that systematic effects related to disk thickness, bulges and bars can produce from mild (10-20)% to severe (30-50)% underestimation of the central circular velocity of galaxies, creating the illusion of constant density

¹Recent results from the 3rd year WMAP revision favor a smaller value of $\sigma_8 = 0.77$ making the concentration found by Swaters et al. (2003a) closer to Λ CDM predictions. See section 5.

cores, while the actual density distribution is cuspy. Similar conclusions were reported by Hayashi et al (2004b). In this case, the effect is associated with triaxial dark matter halos which produce disk ellipticity.

Recently, Simon et al. (2005), and Begum et al (2005) reported results for low mass galaxies consistent with cuspy dark matter halos. In particular, Simon et al. (2005) found evidence for significant radial motions or elliptical streaming in some galaxies. They argue that the non-circular motions can be related to halo ellipticity along the disk plane. They also present one galaxy that favors a steep density profile assuming a stellar (M/L) consistent with the stellar population theory. Spekkens, Giovanelli & Haynes (2005) showed that systematic effects associated with long-slit observations are able to reproduce the distribution of slopes obtained in actual observations of low mass galaxies with no clear evidence for bars or bulges. Dutton et al. (2005) discussed uncertainties in the stellar M/L ratio, halo triaxiality, and distance. They argued that those uncertainties may produce strong degeneracies, making estimates of halo central density less certain. Dutton et al. (2005) also presented estimates of the stellar M/L based on the B-R color and the stellar population models of Bell & de Jong (2001) and another estimate based on the maximum disk solution. Dutton et al. (2005) found that a disk contribution to the circular velocity based on the B-R color of NGC5585 is *above* the maximum disk solution. This suggests that the gas in the center of this galaxy is not supported only by its rotation. Note that internal reddening can produce similar results (Dutton et al. 2005).

To summarize, uncertainties in measurements and interpretation of rotation curves can be quite substantial. In some cases cuspy dark matter profiles provide acceptable fits; in other cases the cusps are problematic. Systematic errors are the most difficult part of the problem. Models, which are disfavored by large χ^2 , can have circular velocities deviating by $\sim 10\%$ from the best-fit models. It is essential to carefully model and understand the systematics in order to decide if there is a conflict with cosmological predictions. In this paper we will focus on two types of systematic effects, that make the rotation velocity differ from the circular velocity: the pressure support and the elliptical motions. We also consider the projection effects discussed in Rhee et al. (2004).

Because some galaxies are consistent with cusps, the heat of debate of cusps vs. cores shifts to those galaxies for which the discrepancy with cosmological predictions is so large that it seems impossible to explain the observed kinematics with a cosmologically motivated halo even considering the uncertainties in the parameter estimation (e.g., Blais-Ouellette, Amram, & Carignan 2001; Moore 2001; Wel-drake et al. 2003; Simon et al. 2005; Dutton et al. 2005). The Magellanic-type galaxy NGC 3109 is the prototype of this kind of system. The galaxy is located at the outskirts of the Local Group. NGC 6822 is another Local Group member of this type. Because of their nearby location, both galaxies have been subjects of high resolution studies, including their kinematics. In order to illustrate the degree of disagreement with cosmology, we quote Wel-drake et al. (2003), who find that a model

of NGC 6822 with a realistic DM halo gives an outstandingly bad fit: $\chi^2_{\text{reduced}} = 1200$. The goal of this paper is to design relatively detailed models for NGC 3109 and NGC 6822, and use the models to evaluate the severeness of the conflict that they pose for the Λ CDM model.

The standard way of constructing mass models for galaxies is to adjust parameters of analytical functions until the model circular velocity produces acceptable fits to the observed rotation curve. However, this approach suffers from some shortcomings. It is usually difficult to test the self-consistency of models: whether the observed gas and stellar kinematics are consistent with the assumed mass distribution. Disk stability against bar formation is another self-consistency test. These potential caveats are known and have been used before to reduce the model parameter space in rotation curve analysis (Athanasoula et al. 1987; Fuchs et al. 2004). However, these problems are often ignored. It is not infrequent to see in literature that models that explain observed rotation curves have a maximum disk that is likely to be unstable for bar formation. In other situations, axisymmetric models are used to explain the kinematics of barred LSB galaxies, as pointed by Swaters et al. (2003b). In many of these cases, questionable results are taken as an evidence for cored halos.

Motivated by all these caveats and by the frequency of non-circular motions and non-axisymmetric structures in the observations of dwarf galaxies, in this paper we consider barred models, and study the corresponding non-circular motions. Given that many of the dwarf irregular galaxies

show photometric or kinematic lopsidedness, we also consider this kind of models. In addition, we use the constraints on the stellar mass provided by observed colors of the stellar population. We make high resolution simulations with several millions of particles moving in a self-consistent gravitational field for billions of years, that assure dynamical self-consistency. Once the simulations finish, we “observe” the models closely mimicking procedures applied to real observational data (Rhee et al. 2004). Models constructed in this way include a number of effects, which are normally difficult to account for analytically: projection effects, finite disk thickness, effects related to complex non-circular motions, adjustment of the dark matter to the presence and evolution of baryons. This procedure can be applied to pure gravitational systems, which allow re-scaling and make it possible to fit a specific galaxy.

There are reasons to believe that the rotational velocities of the gas and stars in dwarf galaxies are not very different. Rhee et al. (2004) and Hunter et al. (2002) addressed this issue observationally. They found that in the central ~ 1 kpc region of late-type (nearly bulge-less) galaxies, stellar and gas rotation curves are very similar to each other. At larger distances, gas rotates slightly faster than the stellar component that, as one would naively expect, has some intrinsic velocity dispersion. Judging by the magnitude of the rotational velocity, one expects that in dwarf galaxies such as NGC 3109 the random velocities are small: 10-20 km/s, which is close to the random velocities of HI clouds. Indeed, this is what we find in our simulations. Hence, it is reasonable to use collisionless models. How-

ever, in order to validate our methodology, we also performed state of the art N -body and hydrodynamical simulations. The simulations included a realistic implementation of stellar and supernova (SN) feedback and allow us to study the effects of gas motion in dwarf galaxies.

The paper is organized as follows. In Section 2 we review the observational properties of NGC 3109 and NGC 6822. In Section 3 we present our hydrodynamical models of a dwarf galaxy and compare the gaseous and the stellar kinematics. Models for NGC 3109 and NGC 6822 are presented in Section 4. A discussion of our results is given in Section 5. A short summary of our results is presented in Section 6. Appendix gives more details of gas motion in hydrodynamical models. We also discuss the corrections to the gas rotation velocity necessary to recover the circular velocity.

2. Observational Data

2.1. NGC 3109

NGC 3109 is a Local Group member that has been extensively studied since it is one of the nearest dwarf irregular galaxies. Observational data for the galaxy are presented in Table 1. Mass of gas in NGC 3109 is an important parameter for our models. Barnes & de Blok (2001) estimated the neutral hydrogen mass for NGC 3109 to be $3.8 \times 10^8 M_\odot$ (after correction to the distance to NGC 3109). Mass of molecular gas is more uncertain. Kahabka et al. (2000) found that not more than 60% of hydrogen in NGC 3109 can be in a molecular phase. Based on CO observations Rowan-Robinson et al. (1980) find that more than 10% of HI must be

in molecular phase. If we take that 30% of the total hydrogen is molecular, which is reasonable following Leroy et al. (2005), and use a factor 1.4 to account for helium and metals, the gas mass in NGC 3109 is estimated to be $(10.3 \pm 0.9) \times 10^8 M_\odot$.

Jobin & Carignan (1990) analyzed observations in I-band as well as in radio wavelengths. The I-band photometry shows a change in the position angle and ellipticity of isophotes as a function of radius, suggesting the presence of a stellar bar, in agreement with B-band observations (Carignan 1985). Jobin & Carignan (1990) concluded that the system is globally dominated by dark matter and their favored model requires a halo with a core radius of almost 7 kpc. van den Bosch, Robertson, Dalcanton, & de Blok (2000) fit an NFW model with a central constant density core assuming the stellar $(M/L) = 0$. Finally, Blais-Ouellette, Amram, & Carignan (2001) analyzed the two-dimensional kinematics of NGC 3109 based on high resolution H_α observations. Their best model with a cuspy halo overpredicts the rotation in the central kiloparsec. This model requires a negligible stellar (M/L) ratio and a concentration smaller than one, which is difficult to reconcile with cosmological predictions. Their favored model has a constant density core radius extending up to 2.4 kpc. Interestingly, the size the halo core has decreased as the observations and the analysis have been improved. Given the quality of the observational data in Blais-Ouellette, Amram, & Carignan (2001), it is considered that NGC 3109 presents a serious problem for cosmological models (Salucci et al. 2003).

TABLE 1
OBSERVED PROPERTIES OF NGC 3109 AND NGC 6822

Parameter	NGC 3109	Reference	NGC 6822	Reference
Morphological type	SB(s)m	1	IB(s)m	1
Distance	1.36 Mpc	2	0.49 Mpc	8,9,10
Inclination	$75^\circ \pm 2^\circ$	3	$60^\circ \pm 2^\circ$	8,11
B-band magnitude	-16.35	4	-15.8	11
K-band magnitude			-17.9	8
B-R color	0.8 ± 0.16	5	0.8	8
Exponential disk scale-length r_d	1.2 kpc	4	0.68 kpc	8
Maximum rotational velocity	67 km/s	3,6	55 km/s	8
Mass of neutral hydrogen M_{HI}, M_\odot	$(4.9 \pm 0.6) \times 10^8$	7	1.34×10^8	12,14
Mass of gas, M_\odot	$(10.3 \pm 0.9) \times 10^8$	7,13	2.3×10^8	12,14,15

References. — (1) de Vaucouleurs et al. (1991) (2) Musella et al. (1997) (3) Jobin & Carignan (1990) (4) Carignan (1985) (5) Lauberts & Valentijn (1989) (6) Blais-Ouellette, Amram, & Carignan (2001) (7) Barnes & de Blok (2001) (8) Wadrock et al. (2003) (9) Mateo (1998) (10) Gottesman & Weliachew (1977) (11) Hodge et al. (1991) (12) de Blok & Walter (2000) (13) Kahabka et al. (2000) (14) de Blok & Walter (2006) (15) Israel (1997)

NOTE.—*NGC 3109*: Results were rescaled assuming the distance of 1.36 Mpc; absolute magnitude was corrected for internal absorption (Carignan 1985).

2.2. NGC 6822

NGC 6822 is also a Local Group member and the third nearest dwarf irregular galaxy after the LMC and SMC. Extensive analysis of properties of the ISM and the stellar component for this galaxy has been done by de Blok & Walter (2000); Weldrake et al. (2003); Komiyama et al. (2003); de Blok & Walter (2006). In order to estimate the total gas mass, we use Israel (1997) results on the mass of molecular gas $M(H_2) = 0.4 \times 10^8 M_\odot$ and make a correction for helium and metals. A summary of the observational properties used in this paper is presented in Table 1.

Though the galaxy is classified as barred, it is generally considered as “a rather average and quiescent dwarf irregular galaxy” (de Blok & Walter 2006). This probably explains why Weldrake et al. (2003) used simple models (no bar or any other complications) to fit the HI rotation curve of this galaxy. Their best model with a cuspy dark matter halo assumes a zero stellar mass-to-light ratio and a concentration close to zero, which is hard to justify not to mention that it systematically over predicts the rotation velocity inside the central kiloparsec. A model with a reasonable halo concentration was rejected with very high confidence.

Yet, the galaxy is far from being simple. The stellar distribution shows a short, but rather strong bar, which is prominent in visible light. This is clearly seen in Figure 8 of de Blok & Walter (2006): the distribution of light in the central $10' \approx 1.5$ kpc is misaligned with the HI at large radii. The misalignment is quite large: Hodge (1977) and Cioni & Habing (2005) give the position angle of the bar $PA = 10^\circ$, while

the position angle of the HI disk is about $PA = 125^\circ$ (Weldrake et al. 2003). This bar was considered the main stellar body of the galaxy; it has an exponential profile. However, deeper photometry reveals a fainter blue component tracing the HI distribution (Komiyama et al. 2003). There is also a faint and rounder red stellar component extending to several radial scale lengths (Letarte et al. 2002). The neutral hydrogen and the faint blue stars show a different position angle compared with the stellar bar. The central surface brightness in B-band is 27 mag/arcsec^2 . This is comparable to the surface brightness of large LSB galaxies (Komiyama et al. 2003). All these properties make NGC 6822 one of the nearest barred LSB galaxies. However, the bar has not been considered in previous analyses of NGC 6822 kinematics (Weldrake et al. 2003).

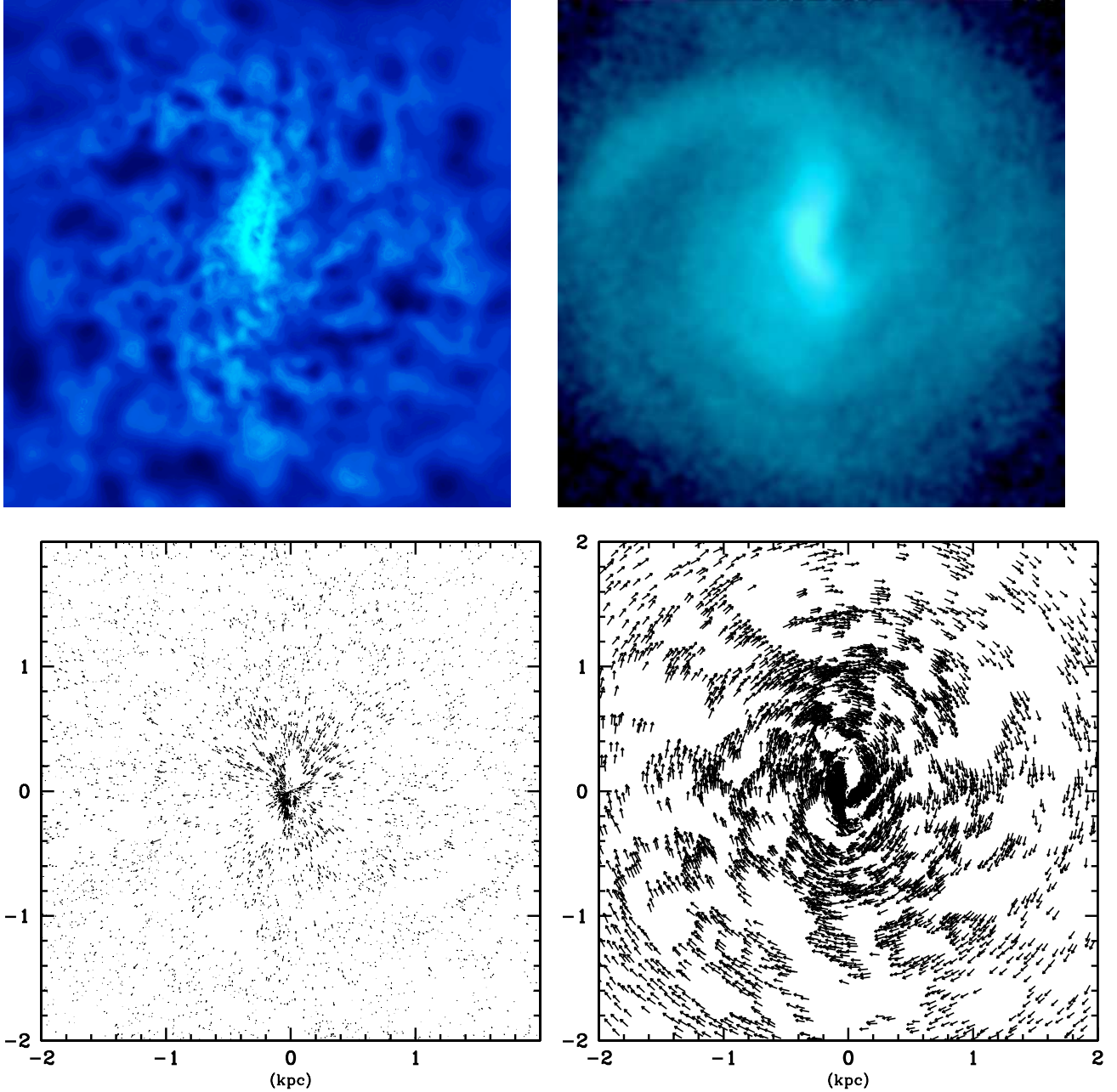


Fig. 1.— The structure and kinematics of the disk in the hydrodynamic simulation. The upper left panel shows the face-on view of cold gas with $T \leq 15000$ K. The cavities are full with a warm gas component that is not shown in the figure ($T \approx (2 - 10) \times 10^4$ K). The upper right panel shows the distribution of the stellar component. Notice that the bar in the gaseous component is weaker and shorter than in the stellar component. The lower left panel shows the radial velocities of cold gas and the lower right panel shows the full velocity field. An arrow with a length of 100 pc corresponds to velocity 60 km/s. The systematic radial motions are clearly present, but their amplitude is low compared to the 42 km/s rotation velocity of the gas at 500 pc and with the 20 km/s value of the rms velocities at the same radius. The upper panels show the projected density along the line of sight. Lower panels present particles in a slice of 20 pc thickness.

3. Kinematics of Gas and Stars: Hydrodynamical simulations.

In order to test the validity of our conclusions based on collisionless simulations (see also Rhee et al. (2004)), we made high resolution hydrodynamical simulations of a dwarf galaxy. These simulations cannot be rescaled because they include gas dynamics and radiative processes. Therefore, fitting them to a specific galaxy is difficult. However, they can shed light on the physical processes playing a role in dwarf galaxies with a significant gas component. In this section we are mostly interested in a simulation, which produced a weak bar because this comes along with what we find in NGC 3109 and NGC 6822. Results of other simulations are presented in the APPENDIX.

The models include a dark matter halo initially with the NFW density profile modified by the standard adiabatic contraction (Blumenthal et al. 1986). The initial parameters of the simulations are presented in Table 2. The models are set initially in equilibrium. The choice of parameters for the simulations was motivated by parameters of NGC 3109 and NGC 6822. The main parameter is the maximum circular velocity. After evolving for 1 Gyr the model had a maximum circular velocity 70 km/s, which is very close to that of the real galaxies. Just as in real galaxies, the disk-to-halo ratio in our models is very small. In next sections we show that our best models for the galaxies have $M_{\text{disk}}/M_{\text{vir}} \approx 0.025$. We selected this value for our hydrodynamical models. Note that this is almost 7 times smaller than the average ratio of baryons to dark matter in a Λ CDM universe. Even with this small

mass the disk makes a significant contribution to the circular velocity in the central 1/3 kpc. Though a reasonable match to real galaxies for some parameters, the hydrodynamical model does not reproduce all the properties of dwarf galaxies. Most notably, the disk is more compact than the disk of the galaxies that we are studying.

The simulations were evolved with the multi-step parallel Tree/SPH code GASOLINE (Wadsley et al. 2004). The code includes hydrodynamics, star formation, radiative and Compton cooling for a primordial mixture of hydrogen and helium as well as stellar and SN feedback. Feedback is modeled as thermal energy dumped into the gas near to star particles. The deposition rate is tied to stellar lifetimes. The affected gas has its cooling shut off for 20 million years, mimicking pressure support from (unresolved) internal turbulence (Thacker & Couchman 2000). The only free parameters (star formation efficiency and the fraction of SN energy dumped into the interstellar medium (ISM) have been tuned over a range of galaxy masses to reproduce a number of observables (Governato et al. 2006; Stinson et al. 2006). Those include the shape and normalization of the Schmidt law of our own Milky Way galaxy and the typical disk thickness, the star formation rates and the gas turbulence observed in small galaxies. Our simulation has initially 2 million particles and has 30 pc softening for gas and stellar component and 60 pc for the dark matter particles. The force is Newtonian at ~ 60 pc. We follow the evolution only for 1 Gyr. Dynamically, this is a very long period for the dwarf “galaxy”: 11 orbital periods at 1 kpc distance.

During the period of bar formation the halo of model H1 is contracted adiabatically due to the disk evolution (Colín et al. 2006). The bar forms very quickly (in about 100 M_{rs}). After that initial period the system is in a quasi-stationary state: Gas show only small radial velocities (see figure 1). Although we analyze the simulation at ~ 1 Gyr there is not a particular reason for that. The model H2 was simulated twice: with and without the star formation. The disk in this model is more extended than in the model H1. As the result, the model is dominated by the dark matter even in the central region. The model did not produce a bar after 1 Gyr of evolution.

Figure 1 shows the structure of the disk as well as the velocity field and radial motions of the cold gas. The distribution of the cold gas is remarkably complex. There is a weak bar, which extends in radius to only 1 kpc. There are spiral arms. At the resolved scales the gas shows a complex structure with cold filaments and holes filled with dilute and relatively hot gas. At these temperatures ($\sim 10^5$ K) and densities the hot gas cools relatively quickly. Consequently, there should be a source of energy and a mechanism to replenish the hot gas. Both are provided by the star formation. The star formation rate $5.5 \times 10^{-2} M_{\odot}/\text{yr}$ is relatively low and is comparable with observational estimates of $(3-6) \times 10^{-2} M_{\odot}/\text{yr}$ for NGC 6822 (Wyder 2001).

Large (100-300 pc) holes and lumps in the distribution of the cold gas observed in Figure 1 are typical for small real galaxies. For example, Figure 8 in Weldrake et al. (2003) shows numerous 1-3 arcmin (100-

300 pc) holes and lumps in the distribution of the neutral hydrogen for NGC 6822. Walter & Brinks (2001) give a catalog of 19 holes with size larger than 200 pc in another dwarf galaxy DDO 47. The same situation – numerous holes, filaments, and lumps – is found in the SMC (Staveley-Smith et al. 1997; Hatzidimitriou et al. 2005), LMC (Kim et al. 1998), Ho II (Stewart et al. 2000). In other words, the multi-phase medium, which we find in our simulation, is characteristic for dwarf irregular galaxies such as NGC 3109 and NGC 6822 studied in this paper.

The observed velocity field in the central ~ 2 kpc region of model is presented in Figure 2. The noisy behavior of contours in the left panel is due to super-bubbles, which induce 5 – 10 km/s motions in the surrounding cold gas. The same kind of “noise” is observed in real galaxies, if observations are done with high resolution. Only after significant smoothing we find a normal “spider diagram” similar to Figure 1 in Swaters et al. (2003a). In this diagram the presence of the bar is a rather subtle effect – a twist of contours in the central 1 kpc area – and can easily be overlooked. Qualitatively the same twist of contours in the velocity field is observed in the NGC 6822 velocity map (Weldrake et al. 2003, Figure 6). In order to quantify the magnitude of the motions, we estimate the rms velocities in different parts of the model. To some degree we follow the observational procedure. In observations the velocity dispersion is often estimated using the gaussian width of emission lines. This is done with some spatial filtering. In order to mimic the observations, we estimate the one-dimensional velocity

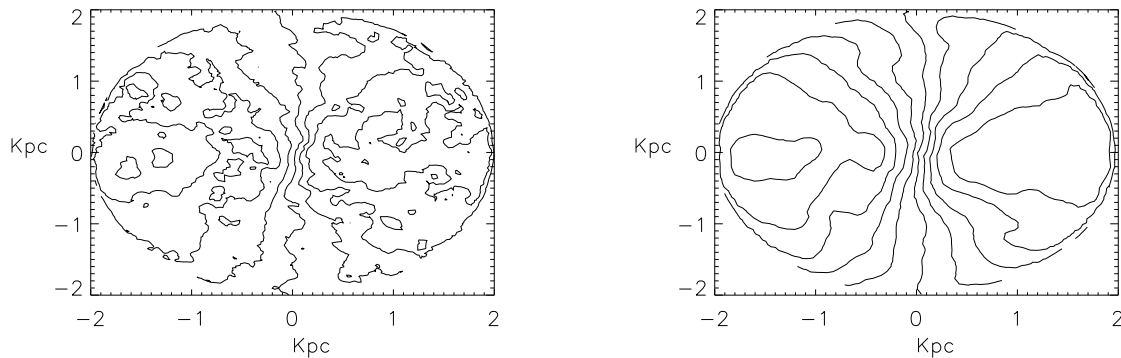


Fig. 2.— The two-dimensional velocity field of cold ($T < 15,000$ K) gas in the hydrodynamic model H1. The figure shows the contours of constant velocity along the line of sight for an observer that measures an inclination of 60° for the galaxy. The left and right panels use different smoothing of the velocity field. The noisy behavior of contours in the left panel is due to super-bubbles, which induce $5 - 10$ km/s motions in the surrounding cold gas. The smoothed velocity field in the right panel shows that kinematic major and minor axis are not orthogonal, which is due to oval distortions related with ~ 1 kpc bar. The bar has a position angle of $\sim 15^\circ$ measured clock-wise from the vertical direction.

dispersion of the cold gas ($T < 15,000$ K). We use different filter sizes (box sizes of 50, 100, and 200 parsecs) to make maps of the observed rms velocity across the whole galaxy. For all cases the average and the most frequent value for the rms velocity in the pixels are 8 and 6 km/s respectively. Thus, local estimates of the velocity dispersion in our model are relatively small and are constant. This is compatible with what is measured in real galaxies at the scale of tens and few hundreds of parsecs (e.g., de Blok & Walter 2000). These values of the rms velocity would normally imply that gas motions are negligible and gas motion faithfully tracks the mass distribution.

Figure 3 shows that this is not true: cold gas rotates slower than expected. The figure presents azimuthally averaged velocities of different components in the model

H1. We show the “true rotation curves” (Rhee et al. 2004): velocities are defined for components in the disk plane. An observer would need to consider in addition projection effects that make the rotation even smaller for most view angles (Rhee et al. 2004) (see section 4 for details). We note that the disk is now a dominant component in the central region of the “galaxy”. The plot shows another important property: the cold gas and the stellar component rotate with similar speeds in the central region, in agreement with the observations reported by Rhee et al. (2004) and Hunter et al. (2002). The main difference between both curves are features related with gas shock waves and an offset of few kilometers per second in amplitude.

It is interesting to apply traditional estimates of the density reconstruction using the rotation curve of the cold gas of the

Model H1. We use the following relation (de Blok et al. 2001) to find the total density $\rho(r)$ when the cold gas moves with velocity $V(r)$:

$$4\pi G\rho(r) = 2\frac{V}{r}\frac{\partial V}{\partial r} + \left(\frac{V}{r}\right)^2. \quad (1)$$

This equation assumes a negligible disk, which is considered as reasonable for LSB galaxies. If the model were treated as a real galaxy, the non-circular motions would be estimated as negligibly small. We already mentioned the rms velocities ≈ 8 km/s estimated using line widths. The average point-by-point variations of velocities also appear to be small: $\approx 10 - 12$ km/s. Adding in quadratures any of those estimates to the “observed” rotation velocity makes very small effect on the rotation curve. For example, at $r = r_d$ the rotational velocity is ≈ 35 km/s. Adding in quadratures 15 km/s gives 38 km/s, which is significantly smaller than the circular velocity of ≈ 60 km/s at that radius. We emphasize that the non-circular velocities only appear to be small. This is how they would be measured by an “observer”. In reality the magnitude of the non-circular motions is larger and their effect is significant. APPENDIX gives more extended discussion of effects non-circular motions and pressure gradients, as well as the corrections necessary to apply to gas kinematics in order to recover the circular velocity.

Figure 4 presents the true density profile and the recovered profile. At distances $r > 3r_d$ the rotation of the cold gas gives a good estimate for the true density in the system. Yet, at smaller radii the cold gas systematically and substantially underestimates the density. We emphasize that

projection effects can make the density underestimation even stronger (Rhee et al. 2004).

In the APPENDIX we give analysis of the discrepancy. We show that the true density can be recovered, but this requires accurate and careful account of numerous effects. Without this, one can get a wrong conclusion that the density in the central region has a core while it actually has a cusp. We also present results of two other simulations (two variants of the Model H2), which address issues of the resolution and the star-formation feedback. In the simulation without the stellar feedback the cold gas rotates very close to the circular velocity of the system. Thus, feedback is definitely responsible for a large fraction of the discrepancy. In the simulation with feedback, but without a bar, the discrepancy is present. Yet, it is not as strong as in the model H1, which has both the feedback and the bar.

We draw two important conclusions from the analysis of the hydrodynamical simulations: (i) the cold gas can rotate slower than the circular velocity. This happens in the central regions of galaxies due to the combined effect of the stellar feedback and a weak bar. (ii) In the central regions the gas rotation and the rotation of the stars are quite comparable. Thus, the stellar motions can be used as a proxy for the cold gas rotation in N-body models.

4. Models for Dwarf Galaxies NGC 3109 and NGC 6822

4.1. N-body Simulations

As we discussed in the introduction, we use N-body simulations in order to model

Table 2: Parameters of Hydrodynamical Simulations

Parameter	Model H1	Model H2
Virial mass M_{200} , (M_{\odot})	2×10^{10}	3.4×10^{10}
Virial velocity V_{200}	40 km/s	40 km/s
Number of dark matter particles	1.7×10^6	2.7×10^6
Number of stellar particles N_{disk}	2×10^5	2×10^5
Number of gas particles N_{gas}	1×10^5	2×10^5
Disk to halo mass ratio	0.025	0.02
Halo concentration C_{vir}	10.	10.
Disk height scale z_d	60 pc	60 pc
Disk exponential scale length r_d	300 pc	600 pc
Disk stability parameter Q	1.2	1.2
Maximum Resolution ($2 \times \epsilon_{\text{star}}$)	60 pc	60 pc

the mass distribution in NGC 3109 and NGC 6822. Our simulations were performed using the parallel Adaptive Refinement Tree (ART) code (Kravtsov, Klypin, & Khokhlov 1997). In this models the disk component is simulated using equal-mass stellar particles. The dark matter halo is sampled with multiple mass species. The halo region surrounding the disk and extending to \sim three times the disk size is sampled with equal-mass particles, each particle having the same mass as that of the “stars”. At larger distances the particle mass increases with radius as described in Valenzuela & Klypin (2003): each subsequent species is twice as massive as the pre-

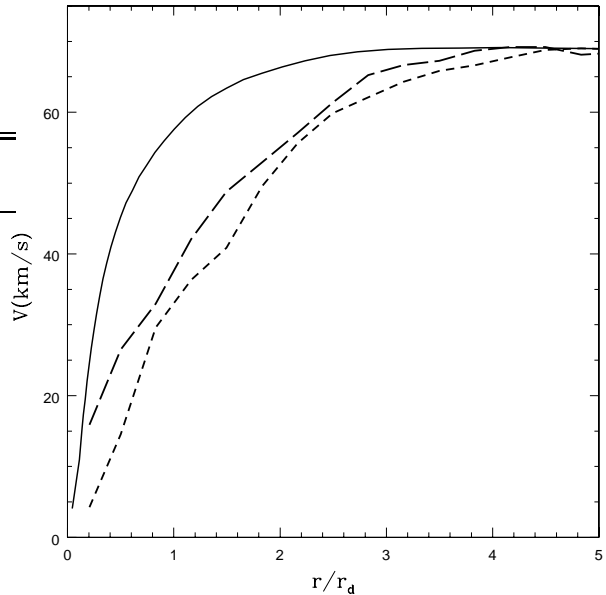


Fig. 3.— Velocity curves in the hydrodynamical simulation H1 of a dwarf galaxy. The full curve shows the spherical averaged circular velocity $\sqrt{GM_{\text{total}}/r}$. The long-dashed curve is for the azimuthally averaged rotation velocity of gas colder than 15000 K. The stellar rotation velocity is shown by the short-dash curve. In the central 1 kpc region the stars rotate slightly slower, but close to the cold gas. Curves for gas and stars are substantially below the circular velocity. At $r > 3r_d$ kpc all the curves are practically the same.

vious one. We use a total of five different mass species for model I and seven mass species for model II. Model I was evolved for 8 Gyrs and model II has evolved for 3.4 Gyrs. Initially the models have only two components: an exponential disk and a dark matter halo with the NFW density profile. The prescription for setting up the initial conditions is described in Valenzuela & Klypin (2003). The initial param-

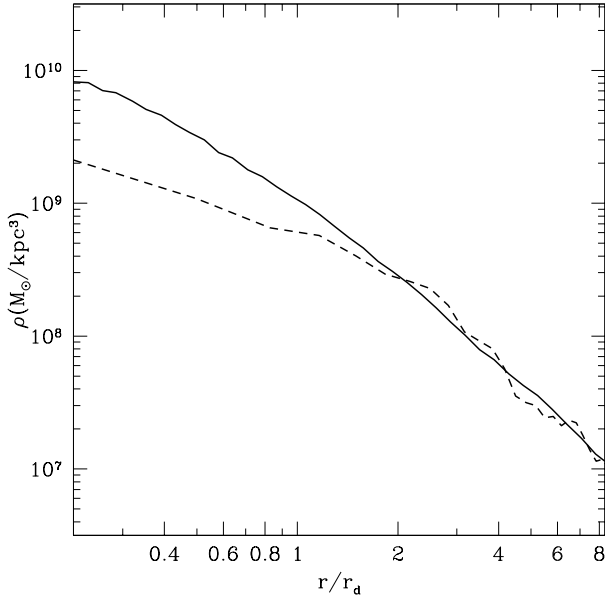


Fig. 4.— Spherically averaged total density profiles for the hydrodynamical simulation H1 of a dwarf galaxy. The full curve shows the true density profile. The dashed curve is the recovered density, calculated from the true rotation curve of cold gas. At large distances $r > 3r_d$ the rotation of the cold gas gives a good estimate for the true density in the system. Yet, at smaller distances the cold gas systematically and substantially underestimates the density. Different effects contribute to the mismatch.

eters of the models and the simulations are shown in Table 3. Model I is based on the model A1 presented by Valenzuela & Klypin (2003), model II was designed from the beginning as a dwarf galaxy.

In addition, the model II was also run to produce lopsided models. There are some motivations to study lopsided models. NGC 6822 shows a tidal tail-like features at large radii. NGC 3109 is also lop-

sided and probably warped. These features may produce additional non-circular motions. We do not try neither to mimic the magnitude of observed lopsidedness nor to investigate the origin of it. We only want to find the effect of the lopsidedness on measured rotation curve. In order to trigger the lopsidedness, we follow the prescription of Levine & Sparke (1998): We displace the disk from the center of the dark matter halo by 0.8 and 2.5 times the initial disk scale length. We then follow the evolution of the system for 3 Gyrs. We call the model with smaller initial displacement “mildly lopsided” and the model with larger displacement “strongly lopsided”.

4.2. Method

The standard procedure used to fit a mass model to a galaxy requires one to vary the model parameters, such as the dark matter halo mass and concentration and the stellar M/L ratio, until the model circular velocity reproduces the observed rotation curve. Disk structural parameters are fixed by the galaxy photometry. In some cases this procedure leads to very small values for the stellar M/L not always in agreement with the observed colors for the galaxy (Blais-Ouellette, Amram, & Carignan 2001). Alternatively, the observed colors of the stellar disk are used in combination with a stellar population synthesis model in order to assign a stellar mass to light ratio (M/L) (e.g., McGaugh 2004). There are some potential drawbacks to this method. The procedure assumes that gas and stars in the disk move with the local circular velocity. However, in many cases there is evidence of non-circular motions in the central regions of

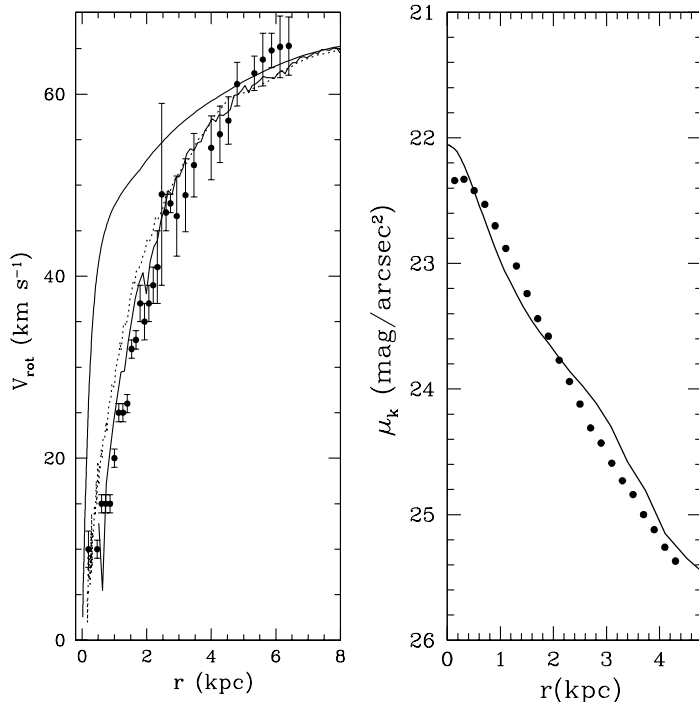


Fig. 5.— Comparison of the model with NGC 3109. *Left panel:* The dots with error bars show the observed rotation curve (Blais-Ouellette, Amram, & Carignan 2001). The lower full curve is the rotation velocity in the model as measured by artificial “observer” placed in such a way that the inclination and position angles match those of the real galaxy (solution of the tilted ring model). The dotted curve does not include effects of projection (azimuthally averaged rotation velocity). The upper full curve show the circular velocity in the model. *Right panel:* Surface brightness in the I band for the actual galaxy (dots) and the model (full curve).

galaxies (Simon et al. 2005; Coccato et al. 2004), which are difficult to take into account. In addition, the hot gas component can give pressure support to the cold gas, as we find in our hydrodynamical simulations. Another potential complication is that parameters of the model are varied freely in order to reach a good fit without any guarantee of self consistency. As a result, the dynamical stability of the model is questionable. In some cases the available observational data give a maximum

disk model that is unstable to strong spiral arms or bar formation. However the kinematics of the model is calculated as if it were axisymmetric, stable and supported only by rotation. This subject has received some attention by Athanassoula et al. (1987) and Fuchs et al. (2004). It is crucial in order to give an accurate interpretation of the observed rotation curves. Even if a galaxy is globally dominated by dark matter, it can develop a strong and healthy bar (Kregel et al. 2005; Athanassoula &

Misiriotis 2002; Valenzuela & Klypin 2003; Debattista et al. 2005). As a result of the instabilities discussed above, the importance of non-circular motions and in some cases the asymmetric drift correction can be under-estimated assuming an exponential, infinitely thin and axisymmetric disk at all radii. Several dwarf and LSB galaxies show deviations from these assumptions particularly in the central regions. The thickness of galactic disks is another issue. It is correctly considered for the calculation of the disk potential (van den Bosch & Swaters 2001). However, it also has a projection effect on the kinematics (Rhee et al. 2004) and possibly in asymmetric drift correction (See Appendix).

We adopted a different modeling procedure that accounts in a realistic way for deviations from axisymmetry and that assures self-consistency. The method is similar to the ones applied to high surface brightness barred galaxies (Kormendy 1983; Athanassoula 1984)). Instead of an analytic rigid model we have a high resolution N-body realization of our system that is evolved for many disk rotation periods. Since gravity is a scale-free force, it is well known that an N-body simulation can be re-scaled using two independent variables. We use this freedom to make the models more realistic. We use the spatial α and velocity γ scales. Thus, if \vec{x} and \vec{v} are the original coordinates and velocities, the rescaled variables are $\tilde{\vec{x}} = \alpha\vec{x}$ and $\tilde{\vec{v}} = \gamma\vec{v}$. Once α and γ are fixed, the mass scale β is defined by $\gamma^2 = \beta/\alpha$.

The first step of the method is to rotate and tilt our model using the observed galaxy position angle (PA) and inclination. Afterward we scale the maximum circular

velocity in the model to the maximum rotation velocity observed in the galaxy, we also change the spatial scale in order to fit the disk radial scale length. The next step is to fix the bar parameters. The radial surface brightness profile is an useful constraint on the strength and length of the bar (Elmegreen & Elmegreen 1985). We use the observed profiles of isophotes ellipticities and PA to fix the bar orientation. This quantity also has a strong influence on the projected surface density.

Bar orientation is an important constraint also for kinematics. It is well known that the effect of non-circular motions on the rotation curve is very sensitive to this parameter (Athanassoula 1984). This effect is larger when the bar is orthogonal to the line of sight and the velocities of many stellar and gas orbits are orthogonal to the observer too. If the orientation of the bar is along the line of sight, the galaxy would appear to have a small bulge and the kinematics would overestimate the circular velocity. However, this galaxy would be considered as consistent with a cuspy halo with a very high concentration, if no modeling of the non-circular motions is performed.

Once the disk and bar orientations are fixed, the standard tilted ring analysis is performed (Begeman 1989). We modify the spatial and velocity scales (α, γ) until we get a satisfactory match between the data points and our model “observed” rotation curve.

We assumed an NFW density profile for the halo. The virial radius is defined as the distance where the halo overdensity is 340 times the average density of the universe. After scaling we have to re-calculate the

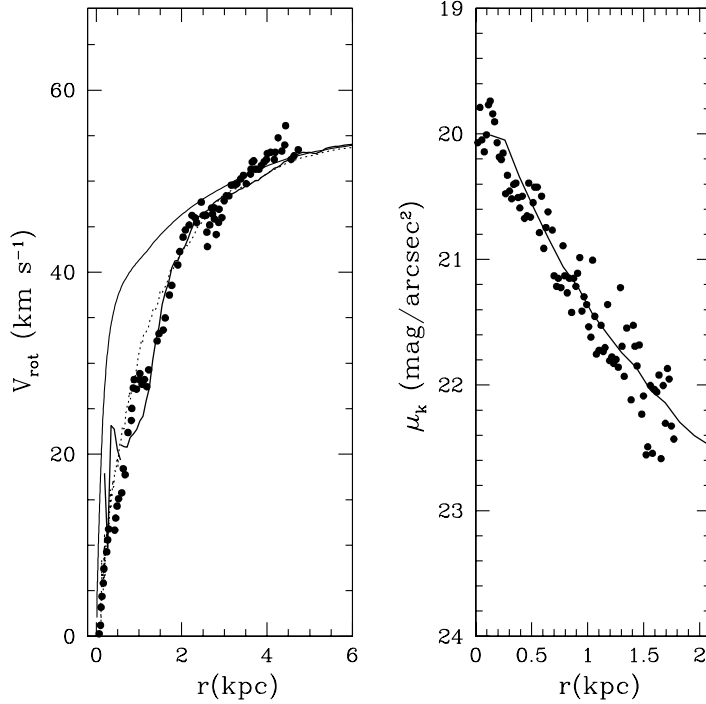


Fig. 6.— The same as in Figure 5, but for NGC 6822. Observational data taken from Weldrake et al. (2003). The right panel shows the unprojected surface brightness in our model (full curve); the dots represent K-band observations from Weldrake et al. (2003).

value of the virial radius. This is done assuming the NFW profile as follows:

$$\frac{3\beta}{\alpha^3 r^3 4\pi} \frac{M_{\text{vir}} F(r/R_s)}{F(C_{\text{vir}})} = 340 \Omega_m \rho_{\text{cr}}, \quad (2)$$

$$F(x) \equiv \ln(1+x) - x/(1+x), \quad (3)$$

where Ω_m the average density of the matter in the Universe, C is the halo concentration, and R_s is the characteristic (core) radius of the NFW profile. The same relation could be written in order to define a relation between the original and scaled quantities:

$$\left(\frac{R'_{\text{vir}}}{R_s} \right)^3 = C_{\text{vir}}^3 \frac{\beta}{\alpha^3} \frac{F(R'_{\text{vir}}/R_s)}{F(C_{\text{vir}})}. \quad (4)$$

Here R'_{vir} is the new (scaled) virial radius, while all the other quantities have the original non-scaled values. The halo characteristic radius R_s is simply multiplied by the spatial scaling factor α . This modifies halo concentration in a non-linear way: $C'_{\text{vir}} = R'_{\text{vir}}/(\alpha R_s)$.

In order to mimic real observations we generated images in FITS format from the stellar disks in our models. The images are processed using IRAF. We use the package STSDAS and the task ELLIPSE in order to define elliptical isophotes over the image. Velocities are projected and integrated along the line of sight of an artificial observer. The isophotes are used for a tilted ring analysis that gives the rotation

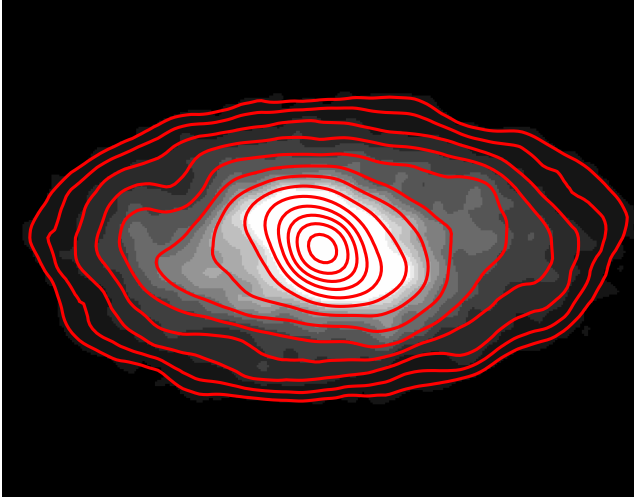


Fig. 7.— The surface density and the isodensity contours for our model of NGC 6822. The projected relative position angle between the bar and the galaxy major axis is consistent with measurements of Cioni & Habing (2005).

curve, the position angle and isophotal inclination profile as a result. This standard analysis assumes that the ellipticity of the isophotes is a measure of the corresponding ring inclination. Our implementation of the algorithm has as an option to assign a global inclination and position angle or to leave these parameters to change as a function of radius. The method is described in detail by Rhee et al. (2004); Begeman (1989).

4.3. Results

We analyze our galaxy model after 3 Gyrs of isolated evolution. At this stage the system evolves very gradually. Its bar slightly grows and slows down. We tried different epochs and selected one which matches the observations. The rotation curve fit is not very sensitive to a particu-

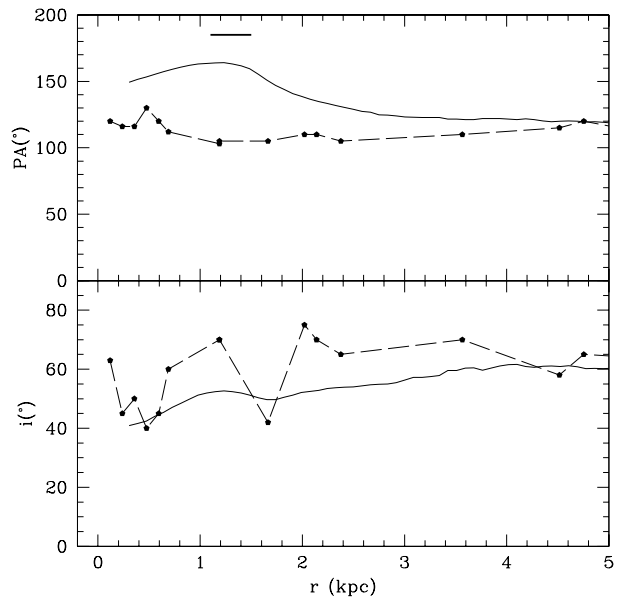


Fig. 8.— Position angle (top panel) and inclination (bottom panel) for NGC 6822. The full curves show results from our model. In the top panel the dashed curve is from observations HI gas (Weldrake et al. 2003). The horizontal line at $PA = 190^\circ$ marks the orientation of the optical bar (Cioni & Habing 2005; Hodge 1977). Note that inside 2 kpc the profile of the position angle in the simulated galaxy shows a change with radius. This change of $\sim 55^\circ$ is consistent with the orientation of the optical bar. The bottom panel shows the “observed” inclination profile calculated using the ellipticity of isodensity curves. The observational data are taken from Weldrake et al. (2003).

lar epoch.

Figure 5 shows the rotation curve of NGC 3109 and compares it with the azimuthally averaged rotation velocity in our model. We also show the surface brightness profile of the galaxy. Assuming that

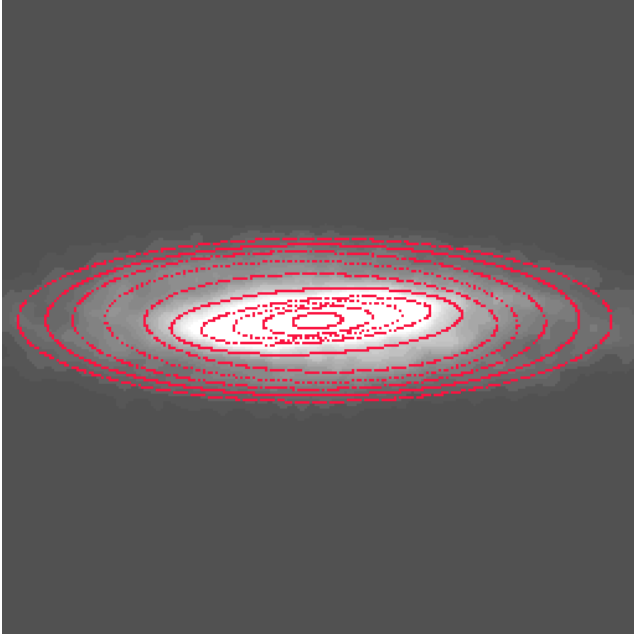


Fig. 9.— Surface density for model of NGC 3109.

mass-to-light ratio does not change with radius, we compare the observed surface brightness with the surface density (scaled to surface brightness units) of the stellar component in the model. Figure 6 shows the same for NGC 6822. When matching the models with galaxies, we adjusted the position of the bars in order to reproduce the gradual change in the isophote orientation presented by Komiyama et al. (2003) for NGC 6822 and by Jobin & Carignan (1990) for NGC 3109. The resulting configuration is in reasonably good agreement with both pictures in the central region. Figures 7 and 8 show the surface density, PA and inclination angle recovered from isophotes for the model of NGC 6822. Figures 9 and 10 present results for NGC 3109.

A striking result, which is apparent in Figures 5 and 6, is that in our models the rotation predicted is smaller than the cir-

cular velocity. This important mismatch between the circular velocities and the observed rotation velocities is due to many effects. In addition to elliptical motions and to the asymmetric drift, there is an extra contribution coming from the fact that our simulated observations average particles at different heights and radii. This projection effect biases the measured velocity toward lower values (Rhee et al. 2004). Note that the non-circular velocities in the models are quite small and are comparable to cold gas motions in our hydro simulation. For example, the velocity dispersion of the stellar component in our models is smaller than 10 km/s for radii larger than 1.5 kpc and it reaches 20 km/s at the very center for the model of NGC 6822. The model for NGC 3109 has a central value smaller than 30 km/s and the amplitude of the rms motions decreases to less than 15 km/s after 1.5 kpc.

Is the mass of the disks in our models acceptable? After all, the baryonic disk is dominant in the central 0.5 kpc in the models. Another issue is the ratio of the disk mass to the virial mass. Our models have a disk-to-halo mass ratio of 2%. This is much smaller than the cosmological baryons-to-dark matter ratio 0.17. Is this a problem? We do not think so. This is comparable to what is observed in real galaxies. For example, for our Galaxy the ratio is (5–6)% (Klypin et al. 2002). In fact, the ratio of 2% is probably realistic but on the high side for dwarf galaxies (Weldrake et al. 2003).

The luminosity, the mass-to-light ratio, and the mass of neutral hydrogen in the disk are other important properties of galaxies, which a model should satisfy.

Knowing the luminosity of the galaxy and assuming a reasonable stellar mass-to-light ratio (consistent with observed colors), we get an estimate of the stellar mass. Observations also provide us with the mass of neutral hydrogen. We can make a correction for the helium to get an estimate of the total gas mass. Mass of molecular gas is still quite uncertain. Observational measurements presented by Leroy et al. (2005) indicate substantial variations in the mass ratio of molecular to neutral hydrogen $M(H_2)/M_{HI}$. In many cases the mass of molecular gas even in dwarf galaxies is comparable with the mass of neutral hydrogen. The sum of the stellar and gas components gives us an estimate of the total mass of the disk. We use this as an additional constraint for our models.

As our fiducial model we adopt one that reproduces the rotation curve and the surface brightness profile and that gives acceptable mass of gas. We also use observational constraints on the total disk mass.

Observational data on luminosity and colors of the galaxies constrain the stellar mass. The B-R color for NGC 3109 is $\sim 0.8 \pm 0.16$ (Lauberts & Valentijn 1989). This implies a stellar $(M/L)_B \sim 0.9 \pm 0.19$ using the models presented by Bell & de Jong (2001). Alternatively, we can use the maximum disk stellar $(M/L)_B \sim 1.5$ (Dutton et al. 2005). Using the mass-to-light ratios and assuming the luminosity $L_B = 5.2 \times 10^8 L_\odot$ we get the stellar mass in the range $4.7 - 7.8 \times 10^8 M_\odot$. The total – stellar plus gas – disk mass in our model of NGC 3109 is $2.1 \times 10^9 M_\odot$. Thus, the mass of the total gas in our model should be $(13 - 16) \times 10^8 M_\odot$. Further assuming that 30% of hydrogen is in molecular

Table 3: Parameters of N -body Simulation.

Parameter	I	II
Number of DM particles	3.3×10^6	1.7×10^6
Mass ratio $M_{\text{disk}}/M_{\text{halo}}$	0.02	0.01
Halo concentration C_{NFW}	15.	14.
Number of disk particles	2×10^5	2×10^5
Disk height-to-length ratio z_d/r_d	0.085	0.1
Stability parameter Q	1.2	1.5
Maximum Resolution ($2 \times$ smallest cell size)	$0.06 z_d$	$0.06 z_d$

form and correcting for helium and metals, we estimate that the mass of neutral hydrogen in the model is $(6 - 8) \times 10^8 M_\odot$. These values for gas mass are somewhat high, but, considering uncertainties, they are still compatible with the masses of different gas components in NGC 3109 (see Table 1). We make the same estimates for lopsided models presented in the next section. Table 4 lists masses of different components in the models.

We now turn to NGC 6822, where the situation is more complicated. Weldrake et al. (2003) gave the K-band luminosity $3.8 \times 10^8 L_\odot$ for the galaxy, but we consider this value as a lower limit. The data covered only the central 1.6 kpc, which produces the luminosity $L_K = 2.4 \times 10^8 L_\odot$ and give a very short exponential length that correspond mostly to the stellar bar. Weldrake et al. (2003) extrapolated the surface brightness profile to larger distances

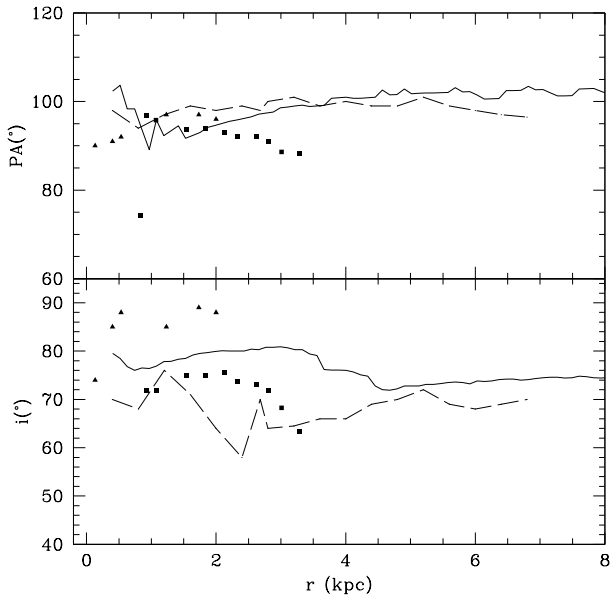


Fig. 10.— Isophotes in NGC 3109. The position angle and measured inclination in the model are presented with full curve. The dashed curve corresponds to the HI data and the squares correspond to the I band isophotes taken from Jobin & Carignan (1990). Triangles represent the H_α observations from Blais-Ouellette, Amram, & Carignan (2001).

using a one-component exponential model. For comparison with our model we will use data only inside 1.6 kpc radius. In our model the mass of the disk inside the radius is $M_{1.6\text{kpc}} = 3.4 \times 10^8 M_\odot$. Assuming $(M/L)_k = 0.5$ for the galaxy, we get stellar mass $M_{*1.6\text{kpc}} = 1.2 \times 10^8 M_\odot$. Thus, our model should have $2.2 \times 10^8 M_\odot$ mass of gas, which is close to the estimated gas mass in the galaxy (see Table 1). Table 4 gives parameters of our model for NGC 6822. Values in parentheses are for central 1.6 kpc. Those should be compared with the observational data in Table 1. Just as for

NGC 3109, we assume that 30% of the total hydrogen is in the molecular form, and we use factor 1.4 to convert from total mass to hydrogen mass.

4.4. Lopsided Models

There are additional complications with the two galaxies besides the stellar bar: NGC 6822 shows tidal tail-like features at large radii and NGC 3109 is lopsided and probably warped. These features may result in additional non-circular motions. In order to test these effects, we produced lopsided models. Figure 11 shows the stellar component and the rotation curves for the lopsided models. Qualitatively results are similar to non-lopsided models. For the lopsided models the underestimation of circular velocity is even larger than for non-lopsided models because the centers of the kinematic and the mass distribution have a different locations, which leads to projection effects. In fact, the disk is not circular any more (Swaters 1999). There are several spiral waves and noncircular motions involved. The main difference with non-lopsided models is that the lopsided models allow more concentrated DM halos. For NGC 3109 we get $C_{\text{vir}} = 11$ for mildly lopsided model and $C_{\text{vir}} = 17.4$ for the strongly lopsided model. When scaled for NGC 6822, the models give even larger halo concentration. We conclude that lopsidedness does not change our main conclusions. It makes them even stronger. Altogether we have four models for each galaxy. Parameters of two lopsided models, which give better fits to observed galaxies, are given in the Table 4.

Our results are not the final models for both galaxies. We still lack reliable ob-

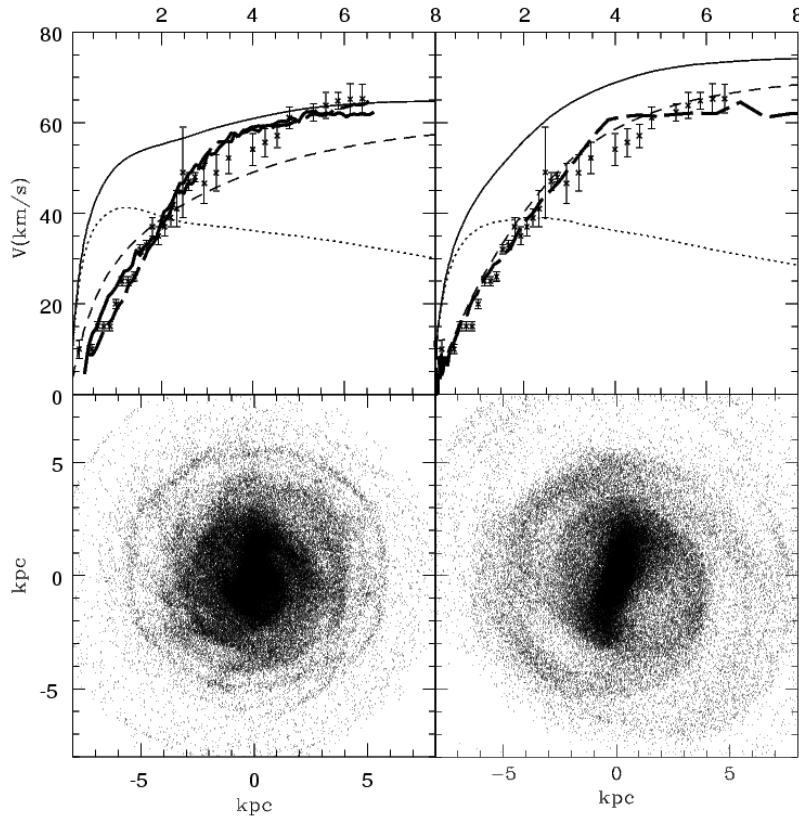


Fig. 11.— Effects of lopsidedness. The left (right) panels are for mildly (strongly) lopsided model II. In the upper panels the circular velocity curves are shown by the top thin curves. Contributions of baryons (dotted curves) and dark matter (short-dashed curves) are also shown. The thick dashed line corresponds to the rotation curve of the lopsided model. As a reference in the left panel, thick solid line represents the rotation curve for the non-lopsided version of the model. Crosses with error bars correspond to the observations of NGC 3109. Lower panels show the corresponding disk particles distribution for both models. For clarity we present particles in a slice of 300 pc thickness.

servational data on the magnitude of non-circular motions and estimates of the effects of the bar and lopsidedness on the kinematics of these galaxies. However, we show that using existing data it is possible to construct a family of models consistent with both cosmological predictions and with the observed properties of the baryonic component. Table 4 gives a

summary of the properties of models for NGC 3109 and NGC 6822.

5. Discussion

5.1. The Tilted Ring Analysis

An important consequence of our results is that the deviations from axisymmetry may and often do bias the recovery of the

distribution of mass in observed galaxies. In the case of NGC 3109 and NGC 6822 these biases are enough to explain the discrepancy between the observed rotation curves and the theoretically expected cuspy dark matter halos. Following previous studies of NGC 3109 and NGC 6822, we allow the PA and inclination to vary during the tilted ring analysis. For a comparison, we also run the analysis fixing these quantities to the average values measured along the disk. We find that the results are sensitive to the assumptions made about the PA and inclination profiles. Our models for PA and inclination are in agreement with observations of Weldrake et al. (2003) and Jobin & Carignan (1990). In our models the changes in PA and inclination are created by the bar.

Our interpretation of NGC 3109 and NGC 6822 as barred galaxies is supported by twists in the isophotes and in the iso-velocity contours (figures 1 and 9 of Jobin & Carignan (1990), figures 5 and 6 of Weldrake et al. (2003), figures 1 and 4 Komiyama et al. (2003)). Many other dwarf galaxies also have variable PA and inclination as a function of radius and, thus, they also may have bars. The standard tilted ring analysis overlooks these variations by interpreting them as warps and assuming that the material out of the disk plane still moves with the local circular velocity which is not obvious (Wong et al. 2004). While warps are definitely frequent in galaxies, warps are believed to be produced by tidal interactions with a companion, a satellite or a triaxial dark matter halo. Those interactions should *increase* with the distance from the center of the galaxy. Yet, the changes in PA and inclina-

tion in NGC 3109 and NGC 6822 happen in the central ~ 1 kpc regions of the galaxies. In the case of NGC6822 the presence of the bar as a feature in the stellar component is evident from the maps of the young stellar component presented by (de Blok & Walter 2006) which is consistent with the central change of PA in the neutral hydrogen and out of phase with the tidal tails. In the case of NGC 3109 the stellar disk seems unperturbed out of one kiloparsec, suggesting that the change in position angle is created by a bar or an oval distortion (Jobin & Carignan 1990). However both possibilities: warps or oval distortions do not exclude each other, making the situation complicated. The ultimate answer will require a detailed modeling of the non-circular motions and the projection effects with methods similar to the ones discussed by Schoenmakers et al. (1997), and it will also require the corrections to the kinematics discussed in the APPENDIX.

5.2. Congruency with Cosmology

Our models reproduce the observed rotation curve as well as some of the disk structural properties of both galaxies. We now evaluate whether the dark matter halos in our models are consistent with cosmological predictions. Figure 12 shows the virial concentration and mass for a population of dark matter halos formed in cosmological collisionless N-body simulations. The amplitude of fluctuations for these simulations was normalized to have $\sigma_8 = 0.9$. Recent results of the third year WMAP revision favor smaller amplitude $\sigma_8 \approx 0.75 - 0.80$ (Spergel et al. 2006), which decreases the predicted average central density of halos. If LSB galaxies are

TABLE 4
MODELS OF NGC 3109 AND NGC 6822

Parameter	NGC 3109	NGC 3109 LOPSIDED	NGC 6822	NGC 6822 LOPSIDED
Virial mass $M_{\text{vir}}, M_{\odot}$	8.1×10^{10}	4.7×10^{10}	3.4×10^{10}	1.93×10^{10}
Halo concentration C_{vir}	14	17.4	22	41
Disk mass $M_{\text{disk}}, 10^8 M_{\odot}$	21.0	15.5	11.0	6.39
Stellar mass $M_{\text{stars}}, 10^8 M_{\odot}$	4.6 – 7.8	4.6 – 7.8	1.9 (1.2)	1.9 (1.2)
Neutral hydrogen mass, $10^8 M_{\odot}$	6 – 8	6.3 – 6.9	4.3 (1.0)	2.1 (1.1)
Total gas mass, $10^8 M_{\odot}$	13 – 16	7.7 – 10.9	9.1 (2.2)	4.5 (2.4)
Stellar (M/L) _B	0.9 – 1.5	0.9 – 1.5		
Stellar (M/L) _K			0.5	0.5
Bar Orientation, degrees	30	30	45	45

NOTE.—*NGC 6822*: Values in parentheses are for inner 1.6 kpc region.

hosted by relatively low concentration halos (Bailin et al. 2005), cosmological predictions for concentration will be reduced almost by a factor of two (Alam et al. 2002, Maccio et al. in preparation). This rescaling will favor our non-lopsided models. However, given that the effect of adiabatic contraction or any possible evolution of the dark matter halo after the disk formation is not included in the relationship between halo mass and concentration, we still compare with the high σ_8 prediction.

The rotation curve and the disk structure of both galaxies – NGC 3109 and NGC 6822 – are consistent with a range of cuspy dark matter profiles. The four models (two non-lopsided and two lopsided) for NGC 3109 are consistent within the uncertainties with the observational estimates of the disk mass. Two of them are within the one-sigma scatter of the average concentration predicted for halos of the corresponding mass. In the case of NGC 6822 the strongly lopsided model II has a concentration well above the average prediction. The non-lopsided version of model II has a relatively small value of the concentration and it is consistent with models discussed by Carigi et al. (2006). In this respect it is remarkable how strong is the effect of lopsidedness, and it also suggests that systematics related with lopsidedness and bars can increase the scatter of concentrations measured using rotation curves.

Yet, not always it produces visible differences. Figure 11 shows the distribution of disk particles in lopsided models. Although the disk shows the asymmetry, the rotation curves are very regular. We can not decide which model – lopsided or not – is better without more accurate obser-

vational data on non-circular motions in NGC 6822. In any case, in all our models the dark matter halos are compatible with predictions of cosmological models.

Figures 11 and 14 present the circular velocity decomposition, showing the individual disk and halo contributions, as well as the combined amplitude. The disk dominates in the central region while the dark matter is dominant in the outer regions. This is typical for barred galaxies (e.g., Athanassoula 1984). This is an important difference with more naive traditional models where the disk is treated as thin and axisymmetric and where the dark matter dominates at all radii. Bar lengths in our models are around 2.4 kpc and 2.0 kpc. The length of bars is reflected in the stellar kinematics, as features in the rotation curves. Still, those features may be difficult to detect because their manifestations are very sensitive to the assumed inclination and position angle that are used in the tilted ring analysis. Because bar lengths in our models are comparable to the outer disk radial scale length, there is a correlation between the size of the region affected by the bars and the disk scale length.

5.3. Generality of our Results

The systematic effects discussed in this paper (see also Rhee et al. (2004)) can affect high accuracy studies of the gravitational potential in galaxies regardless of the specific structure of the dark matter halo or the detailed form of the gravity law. These systematic effects are more exacerbated for non-axisymmetric (barred or lopsided) disks however, they are also present in axisymmetric disks.

Our results regarding NGC 3109 and

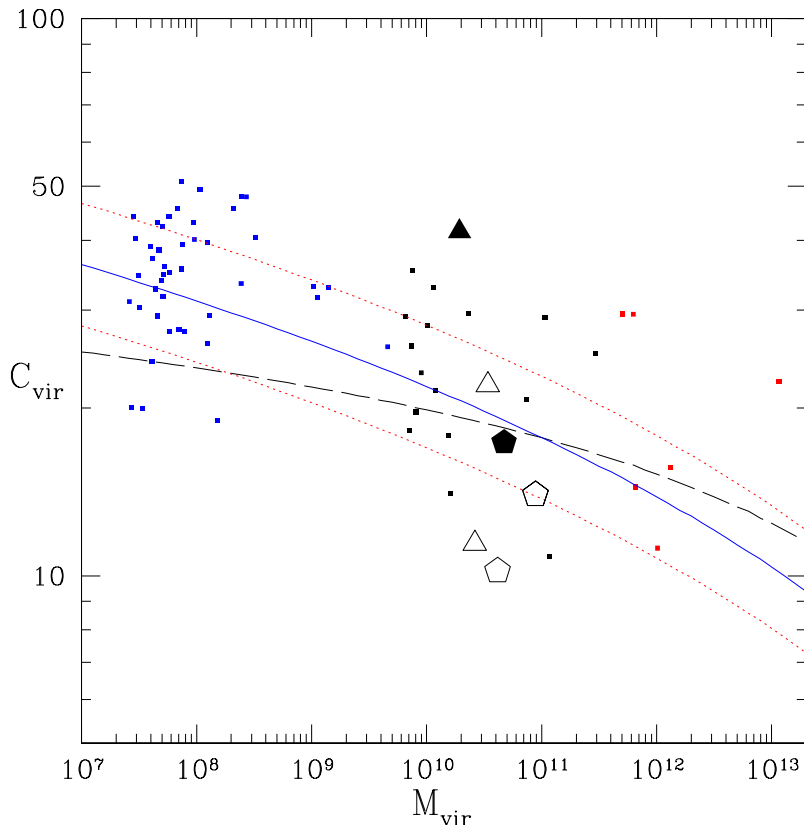


Fig. 12.— Comparison of halo concentrations for three of our models with cosmological predictions. Virial concentrations of our models are shown by large symbols. Models represented by open symbols are not lopsided. Pentagons corresponds to NGC 3109 models, triangles are for NGC 6822. The small squares show the virial mass and concentration measured for halos in cosmological N-body simulation (Colín et al 2004). The central thick line is the model for the relationship between virial mass and concentration proposed by Bullock et al. (2001), thick line is the mean value and the dotted lines indicate the 1 sigma scatter. The dashed line is the model from Eke et al. (2001). The halos in all our models are comparable to those found in cosmological simulations.

NGC 6822, add to the recent arguments of Rhee et al. (2004), Simon et al. (2005) and Spekkens, Giovanelli & Haynes (2005) that some well studied galaxies and the galaxy population on average are consistent with cuspy dark matter halos. Galaxies in our study have been considered impossible to reconcile with Λ CDM cosmology

and previous analysis motivated to explore the modification of dark matter properties or gravity at low acceleration values, or alternatively the galaxies were considered an indication of a crisis for CDM cosmology. (Moore 2001; Salucci et al. 2003; Avila-Reese et al. 2001; Colín et al. 2002).

It is known that both galaxies cannot be treated as simple axisymmetric disks (de Vaucouleurs et al. 1991; Carignan 1985; Hodge et al. 1991). We show that these asymmetries are enough to bias previous analysis toward models with central flat cores.

Our hydrodynamical simulations indicate that because of their low mass, the kinematics of the cold gas in dwarf galaxies is likely affected by pressure gradients triggered by stellar feedback. Once we include these effects in the analysis, the galaxies can be consistent with cuspy dark matter halos. Many of the most discrepant cases like NGC 3109, NGC 6822, IC2574, LMC, and probably DDO47 show bar-like structures, lopsidedness and a large number of shells in their ISM. Our conclusions should be applicable at least to some of them. Finally, we found that estimations of the gas velocity dispersion at scales of tens or a few hundreds of parsecs may underestimate the amplitude of the asymmetric drift correction for galaxies that show non-circular motions.

It has been recently argued that including the adiabatic contraction and a realistic stellar M/L motivated by stellar population models makes the baryonic mass contribution in the center of LSB galaxies to be important (McGaugh 2004). This seems to be at odds with common expectations that LSB galaxies are totally dominated by the dark matter. We emphasize that often those expectations are not based on any solid arguments. Our models support the idea that in the central regions of LSB galaxies the baryons cannot be neglected. The important implication of this picture is that the galaxies are dynamically

unstable to bar and spiral arm formation, creating non-circular motions that lead to the underestimation of the circular velocity.

As a possible solution to the cusp problem of Λ CDM cosmology, it has been suggested that the angular momentum transfer into dark matter halos by galactic bars and satellites can trigger the formation of a flat core (e.g., Holley-Bockelmann et al 2003; El-Zant et al. 2004). Currently there is a discussion about the efficiency of such processes. We can not discard these mechanisms, and kinematic studies of galaxies might help to set constraints to the potential evolution of the dark matter profile. However, given that the effects created by bars – lopsidedness, projection effects and pressure gradients – were not considered before, the evidence for a flat core may be considerably weaker than it has been assumed.

A crucial test for our models of NGC 3109 and NGC 6822 would be a measurement of stellar random motions and non-circular motions in the central region of these galaxies. Blais-Ouellette, Amram, & Carignan (2001) present the H_α velocity field for NGC 3109 in their Figure 2. It is possible to see fluctuations in the velocity field of about 20 km/s. The kinematic fluctuations detected in H_α are consistent with our models, given that the kinematics of ionized gas is likely correlated with the stellar kinematics (Hunter et al. 2002; Rhee et al. 2004). However, a direct measurement of the stellar kinematic would be a better test. Demers et al. (2006) present stellar kinematics in the spheroid of NGC 6822 that can potentially be combined with the disk kinematics to

set tighter constraints on its dark matter halo.

6. Conclusions

In this paper we present self-consistent numerical models for NGC 3109 and NGC 6822 that reproduce their observed rotation curves and some of the structural properties of their disks. Our high resolution models include a number of effects present in real dwarf galaxies like non axisymmetric dynamics and star formation induced gas turbulence.

Our main conclusions are:

A detailed modeling of the baryonic component and a detailed analysis of the kinematics of the tracer population shows that a constant density core for the dark matter halo is not required to successfully reproduce the rotation curves of even the most problematic cases for Λ CDM, like the galaxies NGC 3109 and NGC 6822. On the contrary, the observed rotation curves of these galaxies are consistent with predictions from Λ CDM and they do not provide undisputed evidence for a central flat core.

Our models are centrally dominated by baryons in agreement with observational estimates of stellar M/L ratios based on stellar population models and the colors of dwarf galaxies (e.g., Simon et al. 2005). In many situations we find that models centrally dominated by baryons are unstable to bar formation, which implies the presence of several biases in the interpretation of the rotation curve. It is therefore important to test the self-consistency of the models used to reproduce galactic rotation curves.

Estimations of non-circular motions and

rotation velocity should carefully take in account projection effects, particularly for not axisymmetric disks, otherwise corrections similar to the asymmetric drift will not recover the circular velocity.

It is possible that other effects such as the halo triaxiality also bias estimates of the amplitude and shape of rotation curves in non-barred galaxies (Hayashi et al. 2004b). If the galaxy is barred, the halo is still prolate in the center. In this case the central halo shape is coupled to the baryonic component and the triaxiality is mutually driven by the disk and the halo component (Colín et al. 2006). If the galaxy is lopsided, the underestimation can be more severe. If the circular velocity is small ($\leq 20 - 50$ km/s), as it happens in the smallest dwarf irregular galaxies and in the central regions of large disk galaxies, the pressure gradients triggered by star formation and feedback also contribute to the underestimation of the circular velocity even if the galaxy is axisymmetric.

Accurate measurements and correct treatment of variations in the position angle and inclination as a function of radius along the galactic disk are in some cases critical to set constraints on the mass distribution using rotation curves. If present (as is often the case), those variations may indicate a bar or an ellipsoidal distortion. Different answers can be obtained adopting different interpretations for the PA and inclination angle profile, if the galactic disk is not axisymmetric (Valenzuela et al. 2006). Here we show that a method of analysis that includes the possibility of non-axisymmetric disks is necessary.

In summary, the main lesson of our modeling of mass distribution in dwarf

galaxies is that those galaxies, which were considered as simple dark matter dominated objects with thin cold rotating disks, are actually quite complicated. Efforts to treat them in an overly simplified way result in substantial errors. We find that those errors always *underestimate* the true density in the central parts of galaxies. If confirmed, our results suggest that there is no contradiction between the observed rotation curves in dwarf galaxies and the cuspy central dark matter density profiles predicted by the Cold Dark Matter model. Accurate constraints on halo density profiles will require the modeling of the systematic effects discussed in this paper.

O. Valenzuela acknowledges A. Bosma, E. Athanassoula, J. Gallagher, J. Navarro, M. Tavares, J. Simon, V. Avila-Reese, S. Faber, G. Lake, F. van den Bosch, L. Carigi, P. Colín, G. Gentile, A. Maccio and many others for valuable conversations. F. Governato is Brooks fellow. O. V. acknowledges support by the NSF ITR grant NSF-0205413. A.K. acknowledges support by the NSF AST-0407072 grant to NMSU. Computer simulations presented in this paper were performed at the National Energy Research Scientific Computing Center at the Lawrence Berkeley National Laboratory and also at the Pittsburgh Super Computer Center, using lemieux.

REFERENCES

- Alam, S. M. K., Bullock, J. S., & Weinberg, D. H. 2002, *ApJ*, 572, 34
- Athanassoula, E. & Misiriotis, A. 2002, *MNRAS*, 330, 35
- Athanassoula, L., 1984, *Physics Reports*, Vol 114, Numbers 5 & 6, 319
- Athanassoula, E., Bosma, A., & Papaioannou, S. 1987, *A&A*, 179, 23
- Avila-Reese, V., Colín, P., Valenzuela, O., D’Onghia, E., & Firmani, C. 2001, *ApJ*, 559, 516
- Bailin, J., Power, C., Gibson, B. K., & Steinmetz, M. 2005, *ArXiv Astrophysics e-prints*, arXiv:astro-ph/0502231
- Barnes, D. G. & de Blok, W. J. G. 2001, *AJ*, 122, 825
- Begeman, K. G. 1989, *A&A*, 223, 47
- Begum, A., Chengalur, J. N., & Karachentsev, I. D. 2005, *A&A*, 433, L1
- Bell, E. F. & de Jong, R. S. 2001, *ApJ*, 550, 212
- Blais-Ouellette, S., Amram, P., & Carignan, C. 2001, *AJ*, 121, 1952
- Blumenthal, G. R., Faber, S. M., Flores, R., & Primack, J. R. 1986, *ApJ*, 301, 27
- Bullock, J. S., Kolatt, T. S., Sigad, Y., Somerville, R. S., Kravtsov, A. V., Klypin, A. A., Primack, J. R., & Dekel, A. 2001, *MNRAS*, 321, 559
- Burkert A., 1995, *ApJ*, 477, L25
- Carigi, L., Colín, P., & Peimbert, M. 2006, *ApJ*, 644, 924
- Carignan, C. 1985, *ApJ*, 299, 59
- Cioni, M. R. L., & Habing, H. J. 2005, *A&A*, 429, 837

- Colín, P., Valenzuela, O., Klypin, A.A., 2006 *ApJ*, 644, 000.
- Colín, P., Avila-Reese, V., Valenzuela, O., & Firmani, C. 2002, *ApJ*, 581, 777
- Coccato, L., Corsini, E. M., Pizzella, A., Morelli, L., Funes, J. G., & Bertola, F. 2004, *A&A*, 416, 507
- Debattista, V., Mayer, L., Carollo, M., Moore, B., Wadsley, J., Quinn, T. 2005, *astro-ph/0509310*
- de Blok, W. J. G., & Walter, F. 2006, *AJ*, 131, 343
- de Blok, W. J. G., Bosma, A. & McGaugh S., 2003, *MNRAS*, 340, 657
- de Blok, W. J. G., McGaugh, S. S., Bosma, A., & Rubin, V. C. 2001, *ApJ*, 552, L23
- de Blok, W. J. G., & Walter, F. 2000, *ApJ*, 537, L95
- de Blok W.J.G., & McGaugh S. S., 1997, *MNRAS*, 290, 533
- de Vaucouleurs, G., de Vaucouleurs, A., Corwin, H. G., Buta, R. J., Paturel, G., & Fouque, P. 1991, Volume 1-3, XII, 2069 pp. 7 figs.. Springer-Verlag Berlin Heidelberg New York,
- Demers, S., Battinelli, P., & Kunkel, W. E. 2006, *ApJ*, 636, L85
- Dutton, A. A., Courteau, S., de Jong, R., & Carignan, C. 2005, *ApJ*, 619, 218
- Eke, V. R., Navarro, J. F., & Steinmetz, M. 2001, *ApJ*, 554, 114
- Elmegreen, B. G., & Elmegreen, D. M. 1985, *ApJ*, 288, 438
- El-Zant, A. A., Hoffman, Y., Primack, J., Combes, F., & Shlosman, I. 2004, *ApJ*, 607, L75
- Firmani, C., D’Onghia, E., Avila-Reese, V., Chincarini, G., & Hernández, X. 2000, *MNRAS*, 315, L29
- Flores R., & Primack J.R. 1994, *ApJ*, 427, L1
- Fuchs, B., Böhm, A., Möllenhoff, C., & Ziegler, B. L. 2004, *A&A*, 427, 95
- Gottesman, S. T., & Weliachew, L. 1977, *A&A*, 61, 523
- Governato, F., Willman, B., Mayer, L., Brooks, A., Stinson, G., Valenzuela, O., Wadsley, J., & Quinn, T. 2006, *ArXiv Astrophysics e-prints*, *arXiv:astro-ph/0602351*
- Hatzidimitriou, D., Stanimirovic, S., Maragoudaki, F., Staveley-Smith, L., Dapergolas, A., & Bratsolis, E. 2005, *MNRAS*, 360, 1171
- Hayashi, E., Navarro, J. F., Jenkins, A., Frenk, C. S., Power, C., White, S. D. M., Springel, V., Stadel, J., Quinn, T., Wadsley, J. (2004) preprint (*astro-ph/0408132*)
- Hayashi, E., et al. 2004, *MNRAS*, 355, 794
- Hodge, P. W. 1977, *ApJS*, 33, 69
- Hodge, P., Smith, T., Eskridge, P., MacGillivray, H., & Beard, S. 1991, *ApJ*, 379, 621
- Holley-Bockelmann, K., Weinberg, M., Katz, N. 2003, (*astro-ph/0306374*)

- Hunter, D. A., Rubin, V. C., Swaters, R. A., Sparke, L. S., & Levine, S. E. 2002, *ApJ*, 580, 194
- Israel, F. P. 1997, *A&A*, 328, 471
- Jobin, M. & Carignan, C. 1990, *AJ*, 100, 648
- Kahabka, P., Puzia, T. H., & Pietsch, W. 2000, *A&A*, 361, 491
- Kim, S., Staveley-Smith, L., Dopita, M. A., Freeman, K. C., Sault, R. J., Kesteven, M. J., & McConnell, D. 1998, *ApJ*, 503, 674
- Klypin, A., Zhao, H., & Somerville, R. S. 2002, *ApJ*, 573, 597
- Komiyama et al. 2003 *ApJ* 490 L17
- Kormendy, J. 1983, *ApJ*, 275, 529
- Kravtsov, A.V., Klypin, A.A., & Khokhlov, A.M. 1997, *ApJS* 111, 73
- Kregel, M., van der Kruit, P. C., & Freeman, K. C. 2005, *MNRAS*, 358, 503
- Lauberts, A. & Valentijn, E. A. 1989, *Garching: European Southern Observatory*, —c1989,
- Letarte B., Dermers S. Battinelli P., & Kunkel, W. E. 2002 *AJ* 123, 832
- Levine, S. E., & Sparke, L. S. 1998, *ApJ*, 496, L13
- Leroy, A., Bolatto, A. D., Simon, J. D., & Blitz, L. 2005, *ApJ*, 625, 763
- Mateo, M. L. 1998, *ARA&A*, 36, 435
- McGaugh, S. S. 2004, *ApJ*, 609, 652
- McGaugh, S. S. & de Blok, W. J. G. 1998, *ApJ*, 499, 41
- Moore B., 1994, *Nature*, 370, 629
- Moore, B. 2001, (astro-ph/0103100)
- Musella, I., Piotto, G., & Capaccioli, M. 1997, *AJ*, 114, 976
- Navarro J.F., Frenk C.S., & White S.D.M. 1997, *ApJ*, 490, 493
- Ostriker, J. P. & Steinhardt, P. 2003, *Science*, 300, 1909
- Rhee, G., Valenzuela, O., Klypin, A., Holtzman, J., & Moorthy, B. 2004, *ApJ*, 617, 1059
- Rowan-Robinson, M., Phillips, T. G., & White, G. 1980, *A&A*, 82, 381
- Salucci, P., Walter, F., & Borriello, A. 2003, *A&A*, 409, 53
- Schoenmakers, R. H. M., Franx, M., & de Zeeuw, P. T. 1997, *MNRAS*, 292, 349
- J. Simon, A. Bolatto A. Leroy, L. Blitz and E. Gates 2005, *ApJ*, 621, 757
- Spekkens, K., Giovanelli, R., & Haynes, M. P. 2005, *AJ*, 129, 2119
- Spergel, D. N., et al. 2003, *ApJS*, 148, 175
- Spergel, D. N., et al. 2006, *ArXiv Astrophysics e-prints*, arXiv:astro-ph/0603449
- Staveley-Smith, L., Sault, R. J., Hatzidimitriou, D., Kesteven, M. J., & McConnell, D. 1997, *MNRAS*, 289, 225
- Stewart, S. G., et al. 2000, *ApJ*, 529, 201

- Stinson, G., Seth, A., Katz, N., Wadsley, J., Governato, F., & Quinn, T. 2006, ArXiv Astrophysics e-prints, arXiv:astro-ph/0602350
- Swaters, R. A., Verheijen, M. A. W., Ber-shady, M. A., & Andersen, D. R. 2003, ApJ, 587, L19 , (Swaters et al.(2003a))
- Swaters, R. A., Madore, B. F., van den Bosch, F. C., & Balcells, M. 2003, ApJ, 583, 732, (Swaters et al.(2003b))
- Swaters, R. A. 1999, Ph.D. Thesis
- Thacker, R. J., & Couchman, H. M. P. 2000, ApJ, 545, 728
- Valenzuela, O., & Klypin, A. 2003, MNRAS, 345, 40
- Valenzuela, O., Rhee, G., & Klypin, A. 2006, EAS Publications Series, 20, 83
- van den Bosch, F. C., Robertson, B. E., Dalcanton, J. J., & de Blok, W. J. G. 2000, AJ, 119, 1579
- van den Bosch, F. C. & Swaters, R. A. 2001, MNRAS, 325, 1017
- Walter, F., & Brinks, E. 2001, AJ, 121, 3026
- Weldrake, D. T. F., de Blok, W. J. G., & Walter, F. 2003, MNRAS, 340, 12
- Wadsley, J. W., Stadel, J., & Quinn, T. 2004, New Astronomy, 9, 137
- Wong, T., Blitz, L., & Bosma, A. 2004, ApJ, 605, 183
- Wyder, T. K. 2001, AJ, 122, 2490

7. APPENDIX: Motion of cold gas and the Asymmetric Drift Correction.

In this section we give more detailed analysis of hydrodynamical simulations. We also try to answer some questions regarding gas motion in those models. It is important to clarify that in most cases we will consider the rotation curve measured in the disk plane or the true rotation as in Rhee et al. (2004). An observer should consider the projection effects in order to recover the circular velocity. These projection effects are particularly considerable if the disk is not axisymmetric.

We start with an explanation of why the rotational velocity of the cold gas is significantly lower than the circular velocity as demonstrated by Figure 4. In order to disentangle different effects, we make two runs of model H2 which is axisymmetric and dark matter dominated at each radii: one model includes only hydrodynamics and cooling and the other includes in addition star formation and feedback. Model H2 does not form a bar after one gigayear. So, by comparing these runs we can study the effect of stellar and supernovae feedback in the absence of a bar or an oval distortion.

The left panel in Figure 13 shows different velocity curves for the model H2 without the feedback. It is clear that in this case the cold gas has rotation velocity very close to the circular velocity. This test tells us that numerical effects are not responsible for the disagreement between the rotation and the circular velocities in the model H1. The right panel in Figure 13 indicates that the feedback is partially responsible for the discrepancy: in the model with the feedback the cold gas rotates systematically slower than in the no-feedback model. The difference between the rotation and the circular velocities is about 10% at most radii but it is different inside one radial exponential length. The absolute value of discrepancy is smaller than in the case of the barred model. Still, the effect is definitely present, and it will affect more the slope of the recovered density profile than the average value of the central density. The ten percent difference seems to be small, and one would be tempted to neglect it. Yet, it should not be neglected because another effect goes in the same direction and the cumulative effect of two seemingly small contributions is substantial. Rhee et al. (2004) argued that due to the inclination, the “observed” rotation velocity is slightly smaller than the true velocity. The effect is relatively simple: for a disk with a finite thickness the average 3D radius at which the rotation is estimated is slightly larger than the projected distance. A combination of a rising rotation curve and a projection of the rotation velocity to the line-of-sight results in a smaller “observed” rotation velocity. For a typical inclination of $\sim 70^\circ$ the effect is about 10% (see figs 5 and 7 in Rhee et al. (2004)). The combination of those two effects – projection and feedback – reduce the rotation velocity by at least 20%. When we use eq.(1) to estimate the total density, we find that the “observed” density is only 0.64 of the true density. It is quite remarkable that 10% effects, which normally would be ignored, produce a factor of two underestimation of the total density. This is also a lesson: when dealing with rotation curves every effect on the level of $\sim 10\%$ must be included.

In order to understand other reasons for the disagreement between the large circular velocity $V_c \equiv \sqrt{GM(<r)/r}$ and the small gas rotational velocity V_{rot} , we consider and

estimate different effects related to random velocities and pressure gradients. We can write an equation relating the circular and the rotation velocities of the gas, if we assume that gas with pressure P and temperature T has random bulk velocities with radial dispersion σ_r^2 and velocity anisotropy $\beta \equiv 1 - \sigma_\phi^2/\sigma_r^2$. In this case the analog of the asymmetric drift correction is given by the following expression:

$$V_c^2 = V_{\text{rot}}^2 - \sigma_r^2 \left(\frac{\partial \ln \Sigma}{\partial \ln R} + \frac{\partial \ln \sigma^2}{\partial \ln R} - \beta \right) + \frac{kT}{\mu m_H} \left(\frac{\partial \ln \Sigma}{\partial \ln R} + \frac{\partial \ln T}{\partial \ln R} \right). \quad (5)$$

Here $\Sigma(r)$ is the surface density of the gas, μ is the molecular weight, and m_H is the hydrogen mass. This equation is the Jeans equation in cylindrical coordinates with additional pressure terms. This equation is already a simplification because, as it is usually done, we neglect effects of a possible tilt of the velocity ellipsoid: $\partial \langle v_r v_z \rangle / \partial z = 0$. We also assume that the gas surface density is proportional to the gas density in the plane of the disk. Note that in spite of the fact that gas has isotropic pressure, gas bulk motions in the presence of a bar or an ellipsoidal distortion typically are not isotropic. In all our models the rms velocities in the disk plane are about equal: $\sigma_r \approx \sigma_\phi$. This implies that $\beta \approx 0$. In the model with a bar the rms velocity perpendicular to the disk is about twice smaller than in the plane of the disk: $\sigma_z \approx 0.5\sigma_r$. As a result of this anisotropy in the kinematics the observational estimation of the velocity dispersion in the disk plane will be affected by projection effects.

Left panel in Figure 14 shows contribution of the stellar and the dark matter components to the circular velocity. Here we use spherical approximation to estimate the circular velocity $V_c \equiv \sqrt{GM/r}$. It also shows the rms radial velocity σ_r of the cold gas, this estimation of the velocity dispersion includes small scale random velocities as well as large scale bulk motions created by the bar. We used this estimation of σ_r in eq. (5). Yet, this rms velocity is not what a typical observation would produce. Depending on how the rms velocity is measured in real observations the results can be significantly different. The observed point-by-point rms velocity σ_{los} is a mixture of two contributions: σ_ϕ and σ_z . For example, for an inclination of 45° the “observed” $\sigma_{\text{los}} \approx 0.8\sigma_r$, where we assume that $\sigma_r \approx \sigma_\phi \approx 2\sigma_z$. Even σ_{los} is difficult to measure because of the clumpiness of the ISM in dwarf galaxies and because of the noise in measuring of the velocities. As the result, observers typically report and use average rms velocity for the whole disk. This additionally reduces the value of the rms velocity because a large number of the pixels are in a region out of the bar or oval distortion. If we apply these procedures to our model, we get $\sigma_{\text{los}} \approx (10 - 12)$ km/s.

Results of recovering the circular velocity from the rotation curve are presented in the right panel of Figure 14. To find the circular velocity we use the gravitational acceleration g in the plane of the disk $V_c = \sqrt{rg}$. Just as many observers typically find, we also conclude that the standard asymmetric drift correction makes very little effect. When applying the standard correction, we use the true log-log slope of the surface density of the cold gas and assume a constant rms velocity. In the Figure 14 the crosses are for the standard correction with $\sigma_r = 6$ km/s. Changing this value to 10 km/s does not make any difference. For example, at $r = r_d$ the rotation velocity is $v_{\text{rot}} = 37$ km/s, the circular velocity is $v_{\text{circ}} = 58$ km/s, and

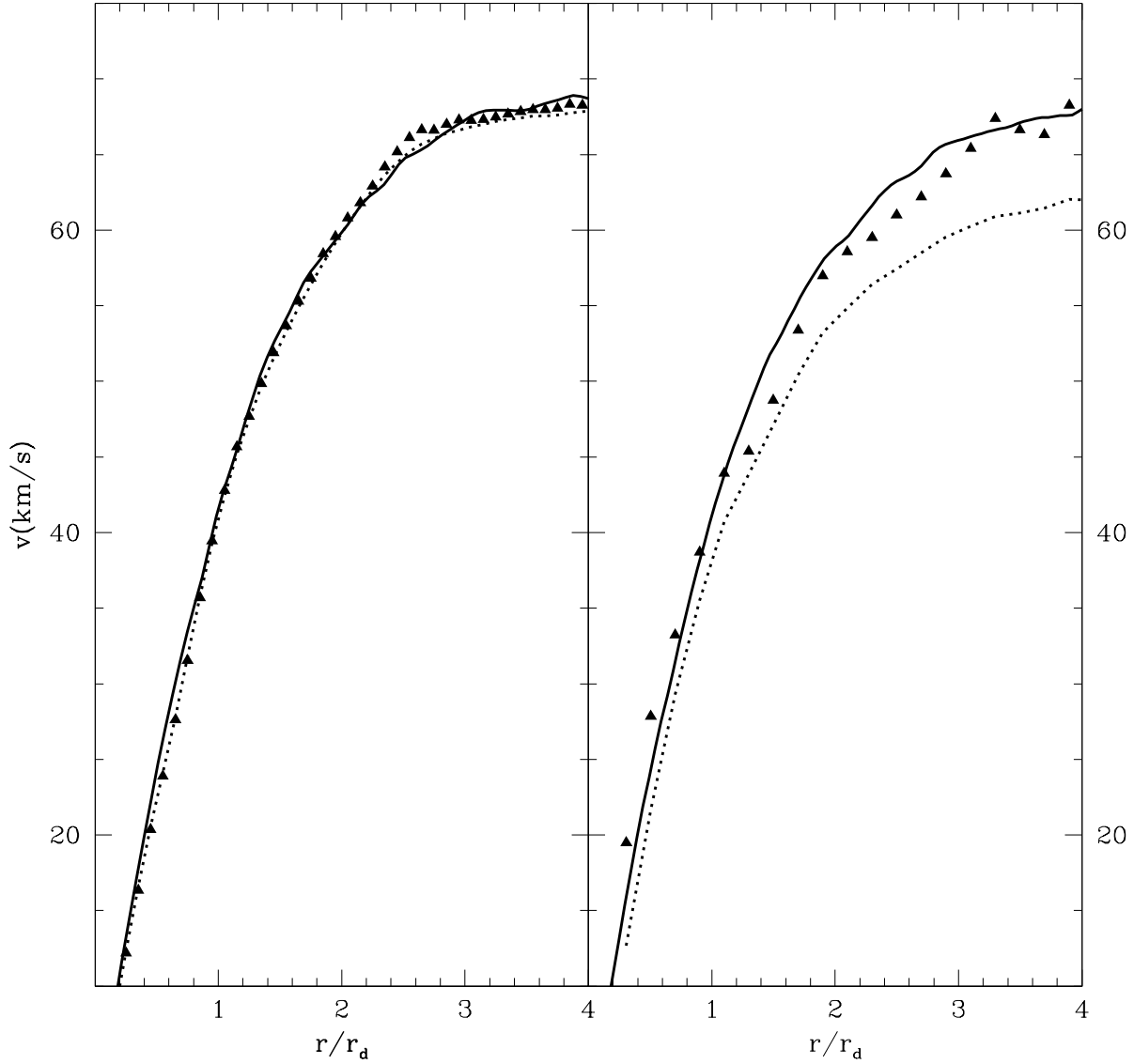


Fig. 13.— The rotational velocity of cold gas (dotted curves) and circular velocity (full curves) in hydrodynamical simulations H2, which do not have a bar. Triangles show results of recovery of the circular velocity from the rotation curve using the asymmetric drift correction. The left panel shows the model with gas cooling but without the star formation. The cold gas rotates very fast and closely follows the circular velocity. The right panel is for the model with the star formation and with the feedback. Gas rotates systematically slower as compared with the circular velocity.

the log-log slope of the surface density is -1.8. If we use $\sigma = 10$ km/s, the correction gives 39 km/s: only a 2 km/s difference! When we use the *true* local rms velocity $\sigma_r = 22$ km/s, we get significantly larger corrected velocity of 47.5 km/s. Still, it does not bring us to the circular velocity, but it is getting much closer. At these small distances there is another factor, which should be included in the correction: the pressure gradient. Effect of only the pressure gradient is shown as the dashed curve in the plot. It makes an impact at all radii, but at $r > 1.5r_d$ it is a small contribution. Yet, at smaller distances it is important. At those distances the mass-weighted temperature of the gas in the plane of the disk is $\approx (20 - 30) \times 10^4$ K. Making all the corrections – for true σ_r and for pressure gradient – gives the corrected value of rotation velocity to 57 km/s, which practically is the true circular velocity. Triangles in the plot show results of application of the corrections at different radii. Indeed, we recover the circular velocity.

We can get additional information about the status of the cold gas by studying forces acting on individual gas particles. If the cold gas is in a quiet rotation, the gravitation and the centrifugal forces should be equal. (Note that the average radial velocity of the gas is close to zero.) The top panel in Figure 15 shows that indeed at large radii ($r \gtrsim 2r_d$) the average gravitational acceleration of a particle is close to its centrifugal acceleration. Yet, at smaller distances the situation is more complex. On average the force of gravity is larger than v_{rot}^2/r . Because on average the gas does not move radially, this means that there is another force, which keeps the particles from falling to the center - the pressure force.

The bottom panel in Figure 15 addresses the issue of the non-gravitational forces in a more direct way: we plot the deviations of the total acceleration g_t from the gravitational acceleration g . Again, on average $g_t \approx g$ at radii $r > r_d$ and there are asymmetries at smaller distances, where on average $g_t > g$. What is quite remarkable about this plot is the magnitude of the scatter. It is important to note that observed a factor of two deviations in the acceleration do not translate to significant deviations in velocities. For example, at $r = 3r_d$ the rms velocity is about 10 km/s – only a 15% deviation as compared with the rotation velocity. At the same distance the force deviations are a factor of three. Here we are looking at the effect of the multiphase medium. Particles of cold gas are pushed by the hot gas and get kicked by supernovae explosions. Yet, particles do not move too far (otherwise they would get large velocities). Before long, they get pushed and kicked again in a different direction.

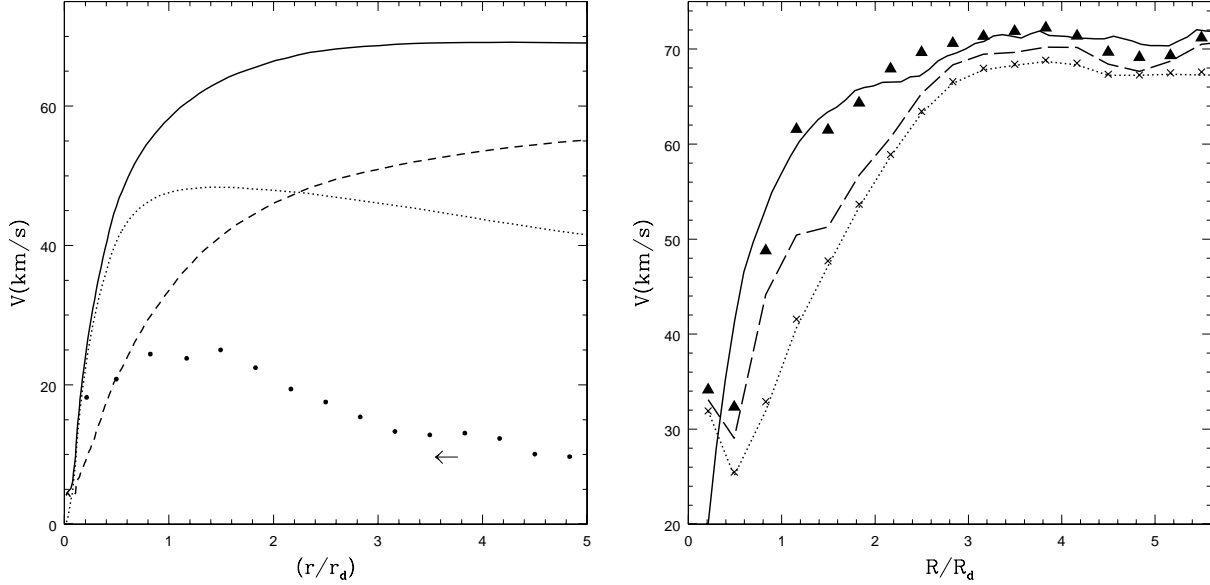


Fig. 14.— *Left*: Velocity curves in the hydrodynamical simulation H1, which has the star formation and a bar. The full curve presents the circular velocity $\sqrt{GM/r}$. The contribution of the dark matter halo is shown by the smooth dashed curve. The dotted curve presents the contribution of the stellar disk. In the central region the disk dominates, while the outer part is dominated by the dark matter. The circles show the rms radial velocity of the cold gas calculated in concentric rings. The arrow indicates the line-of-sight velocity dispersion measured by an observer, which has the resolution of 100 pc and sees the “galaxy” inclined by 40° . Note the difference between the true and observed rms velocities. *Right*: Recovering circular velocity curve in the same model. The full curve is the true circular velocity in the plane of the disk. The rotation velocity is shown by the dotted curve. Crosses show circular velocity recovery results of asymmetric drift correction assuming only a constant rms velocity of the gas 6 km/s. The dashed curve is the recovery results when the only correction term is the gas pressure gradient $(kT/\mu m_H)(d \log \Sigma / d \log r)$. The triangles present results of circular velocity recovery with all the terms included.

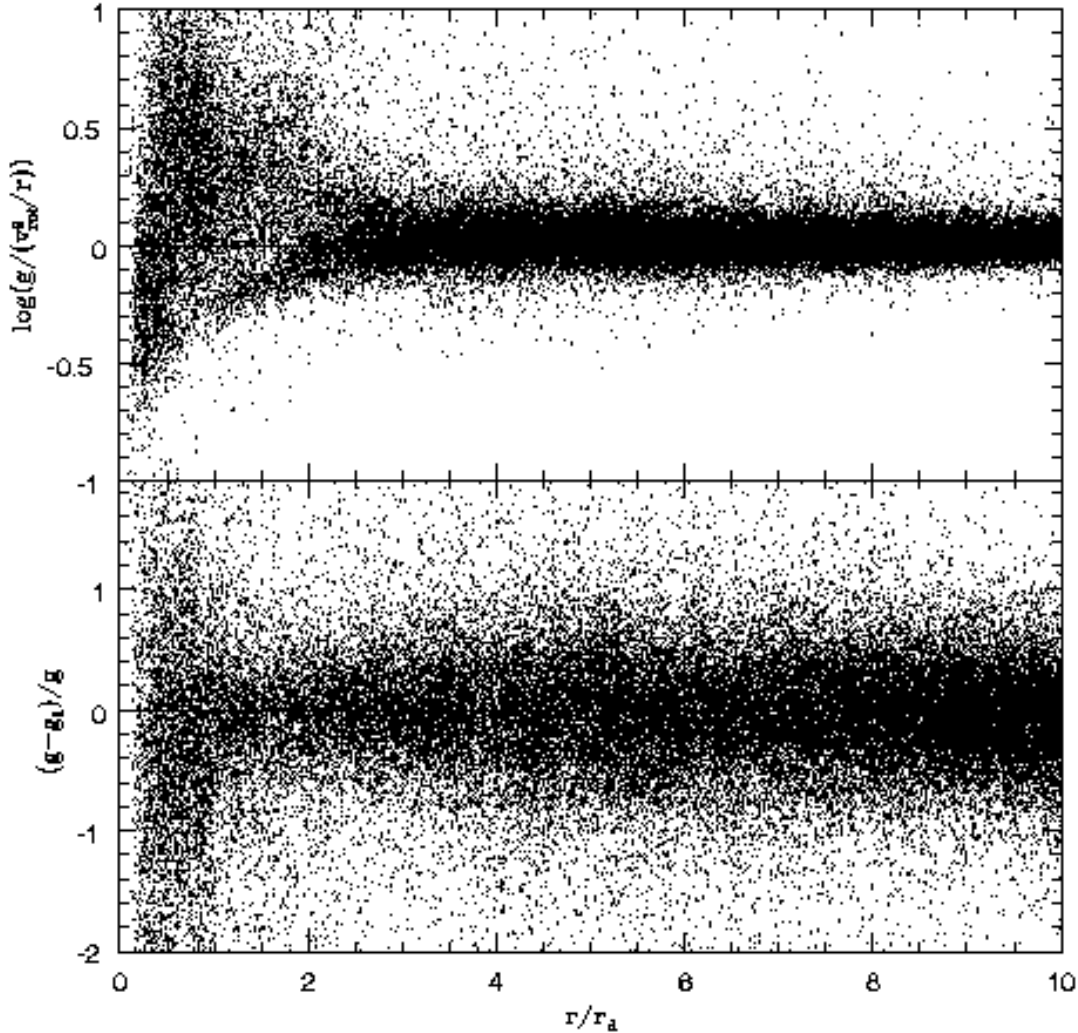


Fig. 15.— Accelerations of individual cold gas particles in the barred model. The top panel shows the distribution of the ratio of radial gravitational acceleration g calculated by the GASOLINE code to the centrifugal force v_{rot}^2/r , where v_{rot} is tangential velocity component of each gas particle. At large distances the ratio is close to unity indicating that fluid elements are close to being rotationally supported. At $r < 2r_d$ the ratio has a large spread and its mean value is larger than unity. Because the average radial velocity of the gas is close to zero, the large ratio means that there is substantial pressure force. The bottom panel shows the fractional difference between the radial component of the total acceleration g_t and the gravitational acceleration g . The scatter shows that there are hydrodynamical forces present.